Lin *et al. Microstructures* **2025**, *5*, 2025070
DOI: 10.20517/microstructures.2024.175

Microstructures

Review

Open Access

Check for updates

The challenge and opportunity of organic semiconductors in photocatalysis

Rui Lin[1], Chou-Hung Hsueh[2], Hongde Yu[3], Thomas Heine[3], Chen Chen[2], Toru Murayama[1]

[1]Institute for Catalysis, Hokkaido University, Sapporo 001-0021, Japan.
[2]Department of Chemistry, Tsinghua University, Beijing 100084, China.
[3]Faculty of Chemistry and Food Chemistry, Technische Universität Dresden, Dresden 01069, Germany.

Correspondence to: Dr. Rui Lin, Institute for Catalysis, Hokkaido University, 10 Chome Kita 21 Jonishi, Kita Ward, Sapporo 001-0021, Japan. E-mail: Rui.Lin@cat.hokudai.ac.jp

How to cite this article: Lin, R.; Hsueh, C. H.; Yu, H.; Heine, T.; Chen, C.; Murayama, T. The challenge and opportunity of organic semiconductors in photocatalysis. *Microstructures* **2025**, *5*, 2025070. https://dx.doi.org/10.20517/microstructures.2024.175

Received: 25 Dec 2024 **First Decision:** 6 Mar 2025 **Revised:** 8 Apr 2025 **Accepted:** 24 Apr 2025 **Published:** 17 Jun 2025

Academic Editors: Sugang Meng, Chunqiang Zhuang **Copy Editor:** Xing-Yue Zhang **Production Editor:** Xing-Yue Zhang

Abstract

Employing organic semiconductors to drive photocatalytic processes for chemical fuel production and pollutant degradation is a viable pathway for tackling the energy crisis and environmental pollution. In this review, we summarize the development of organic semiconductor photocatalysis so far and propose the future vision of organic semiconductors as state-of-the-art photocatalysts in practical applications. Compared to inorganic semiconductors, organic semiconductors display a large absorption coefficient and easily tunable topological and electronic structures, which set them apart from ordinary inorganic photocatalysts. However, the chemical instability, high exciton dissociation energy and low charge carrier mobility of organic semiconductors are the major obstacles to the improvement of their photocatalytic activity. Obviously, the opportunity and challenge coexist in the development of organic semiconductor photocatalysis. In light of this, we systematically compare the merits and shortcomings of organic semiconductors for heterogeneous photocatalysis and enumerate some feasible approaches to overcoming the bottlenecks hindering their photocatalytic performance. By carefully considering factors such as conjugated linkage types, building blocks, and electron donor-acceptor structures, highly reactive and stable organic semiconductor photocatalysts can be developed.

Keywords: Organic semiconductors, heterogeneous photocatalysis, exciton dissociation and diffusion, charge carrier transport, chemical stability

INTRODUCTION

Since clean energy production via the sunlight-driven photocatalytic pathway opened up by Fujishima and Honda[1], great efforts have been made to exploit state-of-the-art photocatalysts for solar fuel production and environmental remediation[2-4]. Up to now, inorganic semiconductors including metal oxides[5], metal oxynitrides[6], metal oxyhalides[7], and chalcogenides[8] are most widely investigated. Photocatalysis involves several key processes, such as light absorption, exciton generation, diffusion, separation, charge carrier transport and recombination, and charge carrier injection to interfacial reactant[9]. Accordingly, structural optimization strategies for inorganic semiconductor photocatalysts have been developed to enhance each of these processes. To enhance the light harvesting and redshift the absorption edge of UV-responsive semiconductors, strategies such as dye-sensitizing[10], quantum dot-sensitizing[11], heteroatom doping[12], solid solution construction[13] are employed. Heterojunction formation[14], defect engineering[15], and crystal facet modification[16] are promising methods to optimize electron-hole separation efficiency and charge carrier dynamics. Nanoparticle size tuning[17] and cocatalyst loading[18] facilitate the charge carriers-involved interfacial chemical reactions. In addition to the traditional inorganic semiconductor materials, other materials with certain intrinsic merits also arouse interest in the community of heterogeneous photocatalysis. Plasmonic nanostructures (Au, Ag, Cu), as a category of photon antennae in solar energy conversion, have recently drawn great attention in photocatalysis owing to their large extinction coefficient and electromagnetic field confinement at nanoscale[19]. The hot carriers with high energy generated after the plasmon dephasing can be injected into the interfacial adsorbed reactant molecules and subsequently trigger chemical reactions[20]. Despite the large absorption cross section and high near-field enhancement in the vicinity of plasmonic nanostructures, in which the electron-electron scattering and electron-phonon relaxation take place at an extremely transient timescale, the lifetime of hot carriers is significantly minimized, resulting in low solar-to-chemical conversion efficiency on the plasmonic nanostructures[21]. Metal-organic frameworks (MOFs), as inorganic-organic hybrid materials with three-dimensional network structures, are also explored for heterogeneous photocatalysis because of their large specific surface area and high porosity[22-24]. The Metal-Oxo clusters isolated by the organic linkers in some MOFs are analogous to semiconductor quantum dots[25], thus endowing corresponding MOFs with semiconductor-like properties[26]. However, a considerable amount of these MOF materials are sensitive to moisture and aqueous solution[25], hindering their further application in photocatalysis. In this context, it is indispensable to develop new classes of photocatalysts to realize the practical application of photocatalysis in energy conversion and environmental remediation.

Why do organic semiconductors arouse great interest in the photocatalysis field?

As stated above, the structure-activity relationship in the inorganic semiconductor photocatalysis has been well established; attention needs to be paid to other promising photocatalysts. Recent years have witnessed the booming progress of organic semiconductor-based optoelectronic devices[27-30] owing to their merit of low cost, flexibility, and facile solution processability. Notably, organic photovoltaic (OPV) has seen substantial advancements, with power conversion efficiencies (PCEs) of single-junction or tandem OPV devices approaching 20%, nearing the PCEs of commercial inorganic solar cells[31]. Considering that the development of inorganic semiconductor photocatalysis draws on a set of methodologies from the inorganic semiconductor solar cells and electronic devices, organic semiconductor photocatalysis could similarly benefit from the recent progress in OPV. Moreover, the fundamental workings of OPV can be divided into light absorption, exciton generation and dissociation, charge carrier transport, and charge carrier collection in organic semiconductor devices[31]. Likewise, organic semiconductor photocatalysis follows the same steps as OPV, with the additional final procedure of charge carrier transfer to reactant molecules. As a result, organic semiconductors are emerging as promising photocatalysts for solar fuel production.

What are organic semiconductor photocatalysts?

Organic semiconductors are a group of organic molecules or polymers with a π-conjugated system constructed by the Pz orbitals of sp2-hybridized carbon or heteroatoms[32]. The transition between π bonding orbital and π^* anti-bonding orbital (π-π^*) has a much narrower energy gap compared to the σ-σ^* transition in the molecules with σ-bonding backbones, endowing the organic semiconductors with visible light response[32]. Up to now, the widely investigated organic semiconductor photocatalysts mainly include supramolecular catalysts[33], conjugated polymers[34], Graphitic carbon nitride (g-C_3N_4)[35], and covalent organic frameworks[36] [Figure 1]. This review paper will focus on the advancement and outlook of organic semiconductor photocatalysis based on these four types of materials.

Supramolecular materials

Supramolecular chemistry is a research field defined as "chemistry beyond the molecule"[37]. As the name suggests, supramolecular formation is an intermolecular assembly via the non-covalent interaction (hydrogen bonding, π-π stacking, dipoles-dipoles interaction, metal-ligand coordination, cation-π interaction)[38,39]. Supramolecular materials have been extensively studied as photocatalysts in recent years [Figure 1A][33], such as porphyrin, phthalocyanine, perylene imide, metal polypyridine complex and their derivatives[40-46]. Inspired by the natural photosynthesis of chlorophylls, porphyrin-based materials have drawn great attention in artificial photosynthesis due to their structural similarity. Porphyrin macrocycles consist of four pyrrole subunits linked by methylene bonds, and these nitrogen atoms in the conjugation system can interact with metal ions via coordination bonds[47]. Based on the chelating interaction between Zn and N, Wang *et al.* realized the self-assembly of porphyrin into supramolecular nanocrystals via a surfactant-assisted synthetic process[48]. Specifically, an acidic solution of H_2TPyP porphyrin derivative was mixed with a basic aqueous solution of cetyltrimethylammonium bromide (CTAB) surfactant. Afterward, adding Zn^{2+} to the mixed solution can chelate the N atoms in the porphyrin macrocycle and thus further results in the formation of ZnTPyP nanowires via a self-assembly process. The as-synthesized ZnTPyP porphyrin supramolecular photocatalyst shows a remarkably high photocatalytic hydrogen production rate. Based on this synthetic protocol, porphyrin derivative supramolecular photocatalysts with different shapes can also be successfully prepared by replacing the surfactant of CTAB[49]. On top of porphyrin-based supramolecular photocatalysts, phthalocyanine is also an important building block for supramolecular photocatalysts because of its excellent light harvesting capability. As another macrocycle with a structure similar to porphyrin, phthalocyanine is made up of four isoindole subunits interconnected via four interval nitrogen atoms, which are also useful for chelating different metal ions. Cu, Co, Zn chelated phthalocyanine supramolecular photosensitizers coupled with TiO_2 show distinct hydrogen evolution rates[50,51], indicating the influence of metal-nitrogen coordination on light absorption and charge carrier transport properties. Additionally, phthalocyanines can also co-assemble with amphiphilic amino acids, forming the supramolecular photocatalysts via π-π stacking and electrostatic interaction. This photooxidase-mimicking vesicular photocatalyst facilitates the oxidation of dopamine into leucodopaminechrome[52]. Generally, porphyrin and phthalocyanine derivatives, as well as other types of supramolecular materials, are excellent photosensitizers and photocatalysts.

Conjugated polymers

Conjugated polymers are a category of macromolecules with π-conjugated main chains composed of repeating building units, which is different from the traditional polymers with saturated main chain structures[53]. The backbones of conjugated polymers are made up of repeating monomers with unsaturated π bonds, such as aromatic, olefinic, or acetylenic building units[34,53]. The mobile π-electrons in the main chain endow conjugated polymers with semiconducting properties[54]. In 1985, Yanagida *et al.* first reported the application of linear polymer poly(p-phenylene) in the photocatalytic hydrogen evolution under 290 nm light illumination[55], opening up a novel era for the conjugated polymer in photocatalysis. Since then,

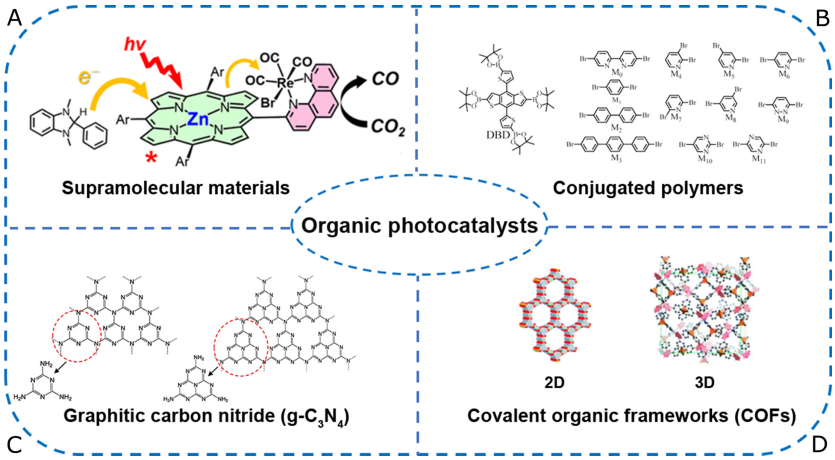

Figure 1. Main organic semiconductor photocatalysts: (A) Supramolecular materials. Adapted with permission[33], Copyright 2020 American Chemical Society; (B) Conjugated polymers. Adapted with permission[34], Copyright 2016 American Chemical Society; (C) Graphitic carbon nitride (g-C_3N_4). Adapted with permission[35], Copyright 2016 American Chemical Society; (D) Covalent organic frameworks. Adapted with permission[36], Copyright 2013 Royal Society of Chemistry. 2D: two-dimensional; 3D: three-dimensional.

multiple attempts have been made to probe the structure-property-activity relationship in conjugated polymer photocatalysis. Extending the oligomer length could redshift the optical absorption edge of 1,4-phenylene/2,5-thiophene copolymers[56]. Furthermore, decreasing the 1,4-phenylene ratio and increasing the 2,5-thiophene ratio in the copolymers can lower the band gap as well. However, a larger 2,5-thiophene ratio lowers the conduction band minimum potential of copolymers, leading to a smaller photocatalytic H_2 evolution rate[56]. Consequently, a trade-off between thermodynamic driving force and optical band gap has to be taken into account when it comes to the molecular design of conjugated polymer photocatalysts. Changing the hydrophobicity or hydrophilicity of the main chain is also a feasible way to tune the conjugated polymers' photocatalytic performance[57]. In addition to the main chain engineering, side chain hydrophilic modification can also boost the photocatalytic activity of conjugated polymers[58,59]. When poly(benzene-dibenzo[b,d]thiophene sulfone) acts as the backbones, the hydrophilic side chain tri(ethylene glycol) shows great advantage in photocatalytic hydrogen production over n-decyloxy and n-dodecyl side chains[60].

Graphitic carbon nitride

Graphitic carbon nitride (g-C_3N_4) is a graphite-like layered carbon nitride material prepared via a simple high-temperature condensation process in an air or inert gas atmosphere using several low-cost, nitrogen-rich precursors, such as cyanamide, dicyandiamide, melamine, thiourea, and urea[35,61]. The condensation of these N-containing monomers can form an in-plane large π-bonded conjugated system arising from sp2 hybridization between C and N atoms. This π-conjugation system in g-C_3N_4 is composed of basic structural units of triazine (C_3N_3) structure and heptazine ring (C_6N_7)[35]. The layers stack via a weak intermolecular interaction with an interlayer spacing of 0.326 nm. As a visible light-responsive semiconductor, g-C_3N_4 shows an optical absorption edge around 450 nm, equaling a band gap of 2.7 eV[61]. The valence band maximum and conduction band minimum energy level of g-C_3N_4 straddles the potentials of corresponding water oxidation reaction and hydrogen evolution, featuring as a promising photocatalyst for water splitting[62]. Since Wang *et al.* discovered the semiconductor photocatalytic performance of g-C_3N_4 in 2009[63], much attention has been paid to exploiting the state-of-the-art g-C_3N_4-based photocatalysts for solar energy fuel production and environmental remediation. Specifically, doping transition metals (Mn, Fe, Co, Ni, Cu)[64] or main group elements (B, S, P) into the skeletons of g-C_3N_4 boosts the photocatalytic activity by narrowing the band gap and enriching the accessible catalytic sites[65-67]. Coupling g-C_3N_4 with

other semiconductors also improves the photocatalytic performance by facilitating the photoexcited electron-hole separation[68].

Covalent organic frameworks

Covalent organic frameworks (COFs) are covalent-bonding crystalline organic porous materials with highly ordered network structures, which are constructed by organic molecular building blocks via condensation reactions[69,70]. Similar to the metal-organic frameworks (MOFs), the two-dimensional and three-dimensional networks of COFs are linked by the nodes and linkers. The corresponding linkage ways vary based on different organic building units, such as boronic acid esters, olefin, triazine, imine, β-ketoenamine, hydrazone, azine, and acrylonitrile, among others[71]. Because of the rigid π backbones, COFs also show semiconductor properties[72] and even have advantages over the other three types of organic semiconductors in some aspects. Compared with organic supramolecules, COFs have a significantly larger specific surface area[73], creating more accessible catalytic sites for photocatalytic reactions. In contrast to the low crystallinity of conjugated polymers, COFs possess a much higher crystallinity, which is beneficial for charge carrier transport[74]. Compared to the triazine- or heptazine-based building units in the g-C_3N_4 structural backbone, the greater structural diversity endows COFs with easier tunable optical and electronic properties[72]. By virtue of so many advantages, COFs have become the most promising organic semiconductors for heterogeneous photocatalysis, as evidenced by the considerable amount of published works since the first reported photocatalytic hydrogen production on TFPT-COF in 2014[75-79].

The advantages of organic semiconductors over inorganic semiconductors in photocatalysis

As mentioned above, organic semiconductors constructed by organic building blocks with large π-conjugation show their promising capability in photocatalytic reactions. In comparison to typical inorganic semiconductor photocatalysts, organic semiconductors exhibit some advantages in the aspects below:

Large absorption coefficient

Light absorption is the prerequisite for photocatalysis and lays the foundation for the subsequent photo-excited charge carrier generation and interfacial catalysis. As a term describing the light attenuation per unit length in a given medium, absorption coefficient can reflect how light was harvested. A high absorption coefficient in a specific material represents that the light beam is mostly absorbed when it passes through the inner space of this material, while a low value indicates that this material has a limited impact on the light beam attenuation. In the layer-by-layer structure of photoelectrochemical working electrode, the thickness of photo-absorbing layer has to be balanced with the thickness of charge carrier mediator layer or catalyst layer[80,81]. A thicker photo-absorbing layer can guarantee high absorption efficiency, but impedes the charge carrier transport in the film or at the catalytic interface[80]. This trade-off strategy works for most of the semiconductors with low absorption coefficients and short charge carrier diffusion lengths. Compared to the typical inorganic semiconductors such as crystalline Si, multiple organic semiconductors possess a much higher absorption coefficient over 10^5 cm^{-1}[82], meaning that thin layer thicknesses can simultaneously facilitate the charge carrier transport without sacrificing the light absorption efficiency, which is conducive for achieving the higher light harvesting efficiency on organic semiconductors. The high light absorption coefficient can be easily achieved on COFs by tuning building blocks with large π-conjugation systems [Figures 2 and 3C].

Facile energy band structure engineering

The energy band structure of semiconductors is of crucial importance for photocatalysis. First and foremost, the band gap of a semiconductor determines which part of sunlight can be absorbed and utilized. As visible light accounts for nearly 43% of the solar spectrum[35], exploiting the visible light-responsive

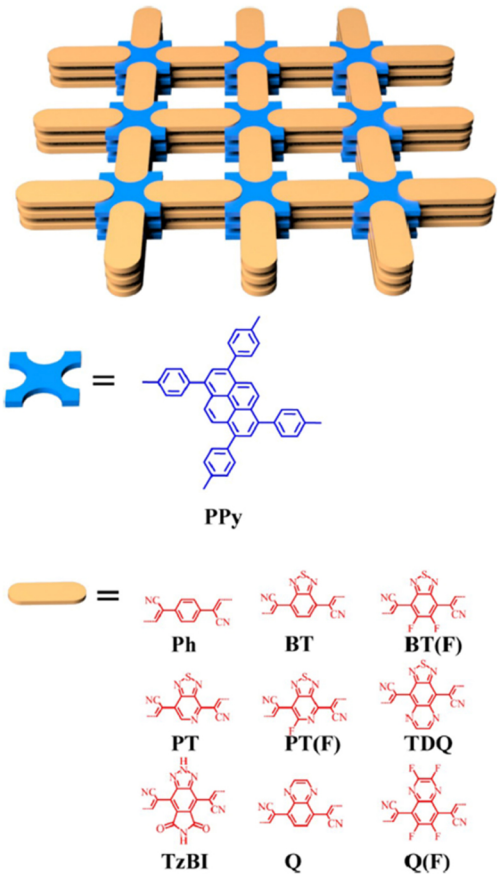

Figure 2. Topological structure and building blocks of stacked 2D COFs of the Lieb lattice with the nodes highlighted in blue and edges in orange. 2D: Two dimensional; COFs: covalent organic frameworks.

photocatalysts is widely accepted as a promising approach for highly efficient capturing of solar energy. Additionally, the conduction band minimum (CBM) and valence band maximum (VBM) energy levels dictate whether the chemical reactions can be initiated thermodynamically. For hydrogen evolution, the potential of the conduction band minimum should be negative compared to the reversible hydrogen evolution (RHE) potential[62]. Designing the solid solution semiconductor is a common approach to redshift the absorption edge of inorganic semiconductors from ultraviolet (UV) to visible light region. For example, the as-synthesized ($Ga_{1-x}Zn_x$) ($N_{1-x}O_x$) solid solution decreases the band gaps of ZnO and GaN from 3.3 to 2.7 eV. However, this nitridation of Ga_2O_3 and ZnO mixture under NH_3 flow takes place at 1,123 K[83]. Nitrogen doping is able to narrow the band gap of TiO_2 as well, but the calcination process still occurs at 823 K under N_2 atmosphere[12]. These harsh synthetic conditions limit the optional inorganic semiconductor materials for photocatalysts and purge us to seek other band gaps tunable materials that can be synthesized under ambient conditions. The band structure of the organic semiconductors is determined by the electron density in the conjugated π-systems and can be manipulated via localizing or delocalizing the π electrons in their conjugation π-backbones[84]. Normally, adjusting the π-conjugation length and changing the substituent groups of organic semiconductors are the two feasible ways to tune the optical band gap, lowest unoccupied molecular orbital (LUMO) and highest occupied molecular orbital (HOMO) energy positions[85-87]. Taking oligothiophenes-based compounds as an example, their band gaps increase from 2.19 to 1.91 and 1.67 eV, with the Thiophene heterocyclic numbers increasing from 3 to 5 and 6. The extension of conjugated π-systems not only narrows the band gap but also upshifts the LUMO and HOMO energy

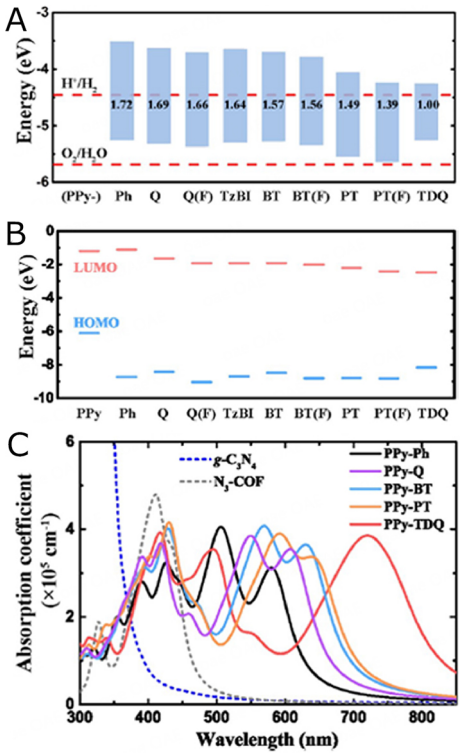

Figure 3. The electronic structure and optical properties of 2D COFs and their related molecular building blocks mentioned in Figure 2. (A) Energy band diagram of COFs; (B) HOMO and LUMO energy level diagram of the molecular building blocks; (C) Absorption coefficients of COFs. 2D: Two dimensional; COFs: covalent organic frameworks; HOMO: highest occupied molecular orbital; LUMO: lowest unoccupied molecular orbital.

levels concurrently[86]. Employing the building blocks (nodes and edges) with different electronic structures also easily enables the band structure engineering of COFs [Figures 2, 3A and B]. When using tetrakis (4-formylphenyl) phenyl as the node, changing the edge structures from phenyl to benzothiadiazole and thiadiazoloquinoxaline results in the shrinking of the band gap because of the extended π-conjugation system [Figures 2 and 3]. The band gap of the related COF remains almost unchanged with the edge building block benzothiadiazole replaced by fluorine-substituted benzothiadiazole, but the HOMO and LUMO positions are lowered because the electron-withdrawing group (-F) decreases the π-electron density of the conjugation system and thus enhances the electron affinity energies[88].

Easy tailoring of dielectric constant

Photoexcited electron-hole recombination via the radiative or non-radiative way is detrimental to enhancing the photocatalytic activity. According to the Langevin formula $\mathrm{R} = \frac{e(\mu_e+\mu_h)}{\varepsilon_r \varepsilon_0} n_e n_h$ (e is the elementary charge, ε_0 represents vacuum permeability, μ_e and μ_h denote the electron mobility and hole mobility, n_e and n_h are the electron and hole concentrations), the electron-hole recombination rate (R) is related to the dielectric constant ε_r of a semiconductor[89]. Therefore, manipulation of the dielectric constant can suppress the electron-hole recombination in semiconductor photocatalysts. Modification of dielectric constants for inorganic semiconductors is only possible by changing their sizes. For example, tuning the diameter of PdS quantum dots from 2.92 to 5.78 nm leads to a noticeable variation in their dielectric constant[90]. On the contrary, the dielectric constant on organic semiconductors can be easily tuned via functional group modification. Poly(3-hexylthiophene) (P_3HT) shows a dielectric constant of 3.75, while the structurally modified sulfinylated P_3HT and sulfonylated P_3AT polymers demonstrate dielectric constants

spanning from 7.4 to 9.3[91]. Moreover, the dielectric constant can be manipulated by changing the structure of organic semiconductors from monomers to dimers and polymers[92]. This dielectric constant improvement relevant to structural modification offers the possibility of lowering the electron-hole recombination rate in organic semiconductors.

Overall, organic semiconductors prevail over inorganic semiconductors in light absorption coefficient, facile modification of energy band structure, and dielectric constant [Figure 4], featuring as an indispensable category of photocatalysts for realizing practical solar fuel production.

How can organic semiconductor photocatalysts be synthesized?

Multiple methods can be used for the synthesis of organic semiconductor photocatalysts. Taking porphyrin-based supramolecular materials as an example, porphyrin monomers can self-assemble into nanostructures via reprecipitation, ion self-assembly, coordination polymerization, and metal-ligand coordination pathways[93]. Using the reprecipitation method, SnIV5-(4-pyridyl)-10,15,20-triphenylporphyrin (SnPyTriPP) and zinc-containing DP($CH_3COSC_5H_{10}O)_2$P porphyrin derivatives can form the supramolecular nanostructures in different solvents[94]. In addition, surfactants, stabilizing reagents, and triblock copolymers can also be used to assist the self-assembly formation of supramolecular well-defined nanostructures[93]. Owing to the electrostatic interactions, supramolecular aggregates can be formed by mixing a cationic porphyrin monomer with an anionic porphyrin monomer. Based on this fundamental, porphyrin nanotubes were successfully prepared by the self-assembly of tin meso-tetra(4-pyridyl) porphyrin cations and tetrakis(4-sulfonatophenyl) porphyrin anions[95]. Concerning the conjugated polymers, their structures are derived from the polymerization of π-conjugated monomers. The aromatic monomers with halogen, alkynyl, amino, carboxyl, and boric acid groups will be interconnected via Sonogashira-Hagihara Coupling, Suzuki-Miyaura Coupling, Yamamoto Coupling, Heck Coupling, Cyclotrimerization Reaction, Phenazine Ring Fusion, Schiff-Base Condensations, Heterocycle Linkages, Alkyne Metathesis, Oxidative Coupling, Buchwald-Hartwig Amination pathways, etc[96]. The typical synthetic processes of conjugated polymers are mixing monomers, catalysts, and solvents under inert gas protection, and then refluxed at a specific temperature for a period of time[97]. The design and synthesis of covalent organic frameworks are similar to that of conjugated polymers. The monomers with different terminal groups undergo the polycondensation processes to form the two-dimensional (2D) or three-dimensional (3D) framework structures. The symmetry of monomers is of great importance, as it determines the topologies and pore sizes of COFs[98]. 2D COFs usually contain planar building blocks and the construction of 3D COFs requires at least one building unit with a tetrahedral or orthogonal geometry[98]. COF materials can be fabricated by various synthetic approaches, such as solvothermal synthesis, microwave synthesis, ionothermal synthesis, and room-temperature solution synthesis[99]. The pristine g-C_3N_4 can be synthesized via thermal condensation of nitrogen-containing precursors including cyanamide, dicyandiamide, melamine, thiourea, and urea at 450-650 °C[100]. Thin-layer g-C_3N_4 can be synthesized by exfoliating bulk g-C_3N_4. Sonication-assisted liquid exfoliation is a promising method to prepare two-dimensional g-C_3N_4 structures, as g-C_3N_4 nanosheets with a thickness of less than 2 nm can be obtained in isopropyl alcohol, 1,3-butanediol, and concentrated sulfuric acid under continuous sonication[101]. Additionally, thermal oxidation exfoliation, ball milling, and flash-freezing methods can also be used to fabricate 2D g-C_3N_4 ultrathin nanosheets[100].

Characterization methods for organic semiconductor photocatalysts

Optical band gap

The optical band gap of organic semiconductors can be measured using a UV-Vis spectrometer. The absorption edge wavelength (λ) of the organic semiconductors is regarded as the absorption onset position in the UV-vis spectra. Accordingly, the band gap of organic semiconductors (E_g) will be calculated based on the equation: $E_g = hc/\lambda$ (h and c denote Plank constant and light speed in vacuum, respectively).

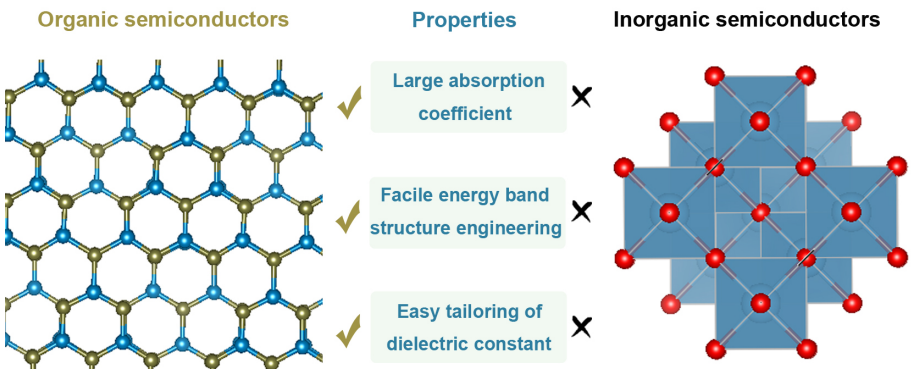

Figure 4. The advantages of organic semiconductors over inorganic semiconductors in photocatalysis.

Energy band potential

HOMO or VBM of organic semiconductors is regarded as ionization energy (IE), which can be measured directly by ultraviolet photoelectron spectroscopy (UPS)[102]. Additionally, LUMO or CBM of organic semiconductors is equivalent to the electron affinity (EA), and the corresponding measurement can be performed via the low-energy inverse photoelectron spectroscopy (LE-IPES) technique on thin-film samples. Moreover, cyclic voltammetry (CV) is also a widely used technique for estimating the IE (or HOMO) and EA (or LUMO) by measuring the redox potentials[103]. CV measurements can be performed both in solution and on thin films.

Dielectric constant

The dielectric constant (ε_r) of organic semiconductors can be measured by impedance spectroscopy at different frequencies[104]. By fabricating a parallel-plate-type capacitor, ε_r of organic semiconductors can be calculated by the equation shown as follows: $\varepsilon_r = C_m d/\varepsilon_0 A$, where C_m, d, ε_0, and A denote measured capacitance, thickness, vacuum permittivity, and area of the capacitor, respectively. The value of C_m can be obtained based on the impedance test $C_m = \frac{-Z''}{\omega|Z|^2}$, where Z, Z'', and ω represent the total impedance, the imaginary part of the impedance, and angular frequency, respectively[102]. Therefore, the exact value of the dielectric constant (ε_r) will be acquired after the determination of measured capacitance (C_m).

Exciton binding energy

The exciton binding energy E_b of organic semiconductors can be determined from the temperature dependence of photoluminescence (PL) measurements[105]. Thermal dissociation of excitons was assumed to fully contribute to the radiative recombination of electron-hole pairs, which can be reflected by PL intensity change. Since the PL intensity decreases with the enhancement of temperatures, the calculation of activation energy in the Arrhenius equation can be extrapolated to the determination of exciton binding energy. Based on this equation: $\frac{I(T_0)}{I(T)} = 1 + Ae^{\frac{-E_b}{k_B T}}$, where $I(T_0)$ and $I(T)$ are the PL intensity at different temperatures, k_B denotes Boltzmann constant, and the slope of the linear fitting of $\ln[I(T_0)/I(T)-1)]$ versus $1/(k_B T)$ corresponds to the exciton binding energy[106].

Charge carrier dynamics

The exciton dissociation of organic semiconductors can be probed by photoluminescence spectroscopy (PL), and the PL emission peak intensity declining at a certain wavelength indicates the exciton quenching[107]. The charge transfer dynamics of organic semiconductors can be investigated via time-resolved photoluminescence (TRPL) technique. PL emission peak intensity decay as a function of time can reflect the lifetime of the photo-excited electron-hole pair. Considering that TRPL mainly monitors the

charge carrier dynamics at nanosecond (ns) timescale, more precise information about charge carrier dynamics in a picosecond timescale can be provided by the femtosecond pump-probe transient absorption spectroscopy (TAS)[107,108]. In this technique, the pump laser beam excites the organic semiconductors, generating excitons, and the probe beam then reaches the excited sample after a delay to trace exciton diffusion and dissociation[108,109].

Photocatalytic reactions for organic semiconductors

Hydrogen evolution reaction

Photocatalytic water splitting is considered a sustainable approach to producing clean hydrogen, which takes place when the conduction band minimum potential of a photocatalyst is more negative than the reversible hydrogen evolution (RHE) potential. Organic semiconductors with tunable energy band structures show their competencies for hydrogen production[110]. Using triethanolamine (TEOA) as a sacrificial agent, g-C_3N_4 was found to be active in hydrogen evolution with a reaction rate ranging from 0.1 to 4 μmol·h^{-1} under visible light illumination[63]. As bulk g-C_3N_4 still suffers from low visible light harvesting, high photo-excited charge carrier recombination, and limited surface catalytic sites, much effort has been made to its structural modification[110]. Doping sodium ions into the skeleton of g-C_3N_4 decreases the band gap of pristine g-C_3N_4 from 2.74 to 2.42 eV[111]. Because of the extended visible light response, as-synthesized Na-doped g-C_3N_4 displays a H_2 evolution rate nearly 4 times higher than that of pristine g-C_3N_4. Moreover, g-C_3N_4 and sulfur-doped g-C_3N_4 can form the staggered gap heterojunction, which is able to separate the electrons and holes efficiently[112]. Compared to the shorter charge carrier lifetime in g-C_3N_4, time-resolved photoluminescence spectroscopy reveals that photo-excited charge carrier lifetime is prolonged in this isotype heterojunction, leading to a H_2 evolution rate 11 times higher than that of pure g-C_3N_4. Furthermore, forming layered nanojunctions with MoS_2 can enrich the surface catalytic sites on g-C_3N_4 for hydrogen production[113]. MoS_2 not only serves as a charge carrier mediator to deliver the photogenerated electrons on g-C_3N_4 to proton, but also reduces the activation energy for hydrogen evolution. Designing mesoporous g-C_3N_4 is also a feasible way to improve the hydrogen evolution activity by enhancing the accessible catalytic sites[114]; this methodology also works for the optimization of covalent organic framework photocatalysts. The hydrophilic 3.2 nm mesopores in fused-sulfone-COF can adsorb dye photosensitizers[115]. Owing to its high specific surface area and wide visible light response, this dye-sensitized COF exhibits a hydrogen production rate of 16.3 mmol·g^{-1}·h^{-1} and an apparent quantum efficiency of 2.2% at 600 nm[115]. As the first reported organic semiconductor photocatalyst for hydrogen production, conjugated polymers undoubtedly have drawn great attention in this field. The hydrophilicity of conjugated polymers was enhanced significantly when the building unit of dibenzo[b,d]thiophene was replaced by dibenzo[b,d]thiophene sulfone, resulting in a remarkably improved hydrogen evolution rate[116]. Additionally, decreasing the particle size of conjugated polymers can also boost the hydrogen generation activity[116]. However, it is still disputable about the hydrogen evolution activity of conjugated polymers because the polycondensation polymerization processes of multiple conjugated polymers are catalyzed by metals, and the trace amount of these residual metals in the conjugated polymers can serve as cocatalysts boosting hydrogen evolution reaction to some extent[117-119]. Control experiments have unraveled that even though purified by Soxhlet extraction, Pd with a concentration smaller than 40 ppm can still reside in F8BT conjugated polymers, thus impacting hydrogen evolution reaction[117]. The long-lived photogenerated electrons in F8BT conjugated polymers can instantly and efficiently transfer to the residual Pd clusters before being injected into protons[118]. Therefore, the excellent photocatalytic activities on a majority of conjugated polymers originate from the synergy of residual metals cocatalysts and conjugated polymers photocatalysts rather than only conjugated polymers themselves. It is still impossible to thoroughly rule out the existence of residual metals in conjugated polymer photocatalysts at the current stage[119].

CO_2 reduction reaction

Photocatalytic CO_2 reduction to useful chemicals or industrial feedstocks has aroused great interest in the community of organic semiconductor photocatalysis[120]. Much attempt has been made to design robust organic semiconductor photocatalysts for CO_2 reduction, but the multiple proton-coupled electron transfer pathways in the reaction result in sluggish kinetics and low product selectivity[120,121]. ACOF-1 constructed by the condensation of hydrazine hydrate and 1,3,5-triformylbenzene generates methanol in photocatalytic CO_2 reduction without any sacrificial agent[122]. HCOF-1 synthesized by the condensation of hydrazine hydrate and 1,3,5-triformylphenol shows the same azine-linkage type as ACOF-1, while producing CO and CH_4 in photocatalytic CO_2 reduction reaction using TEOA as sacrificial agent[123]. Moreover, LZU1-COF formed via condensation of p-phenylenediamine and 1,3,5-triformylbenzene generates only CO in pure water under light illumination[124]. All these results indicate that photocatalytic CO_2 reduction reaction selectivity strongly depends on the building units of the organic semiconductor and the solvent microenvironment. In general, CO, HCOOH, CH_4, CH_3OH, and C_2H_5OH are common products in organic semiconductor photocatalytic CO_2 reduction reactions. CO_2 reduction to CO is the most kinetically preferable pathway because of its lowest quantity of involved protons and electrons[120]. The ultrathin imine-based 2D COF nanosheets (NSs) show excellent photocatalytic CO_2 reduction to CO. Among them, COF-367-Co NSs display a CO production rate of 10,162 $\mu mol \cdot g^{-1} \cdot h^{-1}$[125]. CoO_4 catalytic sites-modified 2,3-dihydroxybenzene-1,4-dicarboxaldehyde (2,3-DHTA)-based COF also shows an extremely high CO generation rate of 18,000 $\mu mol \cdot g^{-1} \cdot h^{-1}$[126], outperforming any other organic semiconductor photocatalysts. Similar to CO production, HCOOH generation also involves the transfer of two electrons and two protons[120]. Metal-nitrogen coordination catalytic sites are proved to be crucial for boosting the formation of HCOOH. The Ru-N_2 incorporated covalent triazine framework (CTF-2) displays a HCOOH generation rate of 2,090 $\mu mol \cdot g^{-1} \cdot h^{-1}$[127], which, to the best of our knowledge, is the highest photocatalytic HCOOH production rate reported among all organic semiconductor photocatalysts. The ketoenamine-based COFs with the same TpBD framework and different functional groups show distinct photocatalytic HCOOH production activity. Functional group -OCH_3 exhibits an advantage over -CH_3 and -NO_2, resulting in a higher HCOOH generation rate for TpBD-$(OCH_3)_2$ COF compared to other COFs[128]. Different from CO and HCOOH production with relatively facile reaction kinetics, CH_4 generation is more difficult on reaction kinetics because of the involvement of eight electrons and protons[129]. By designing a D-A structure between tris(4-ethynylphenyl)amine (TPA) and phenanthraquinone (PQ) to enhance the intramolecular electron transfer, the synthesized TPA-PQ photocatalyst overcomes the sluggish kinetics of CH_4 generation and displays a visible-light-driven photocatalytic CH_4 production rate of 2.15 $mmol \cdot g^{-1} \cdot h^{-1}$[130], which is much higher than that of TEB-PQ (0.268 $mmol \cdot g^{-1} \cdot h^{-1}$) constructed from the building blocks of triethynylbenzene (TEB) and PQ. The production of alcohols via photocatalytic CO_2 reduction is challenging, but can be realized by designing appropriate catalytic sites. Embedding PdIn bimetallic clusters into the pores of N3-COF facilitates the generation of CH_3OH and C_2H_5OH simultaneously[131], resulting in CH_3OH and production rates of 24.5 and 8.75 $\mu mol \cdot g^{-1} \cdot h^{-1}$, respectively. Tan *et al.* introduced N vacancies and O doping to create dual catalytic sites in the skeleton of a melon-based organic photocatalyst[132]. The localized charge polarization in the as-synthesized oxygen-doped and nitrogen-defective melon-based organic photocatalyst (ON-MOP) simultaneously promotes C-C coupling and lowers the exciton binding energy, thus yielding a C_2H_5OH production rate of 800 $\mu mol \cdot g^{-1} \cdot h^{-1}$ with a selectivity of 97%. These state-of-the-art organic photocatalysts in CO_2 reduction are shown in Table 1.

H_2O_2 production reaction

Hydrogen peroxide (H_2O_2) is an eco-friendly oxidant widely used in various fields[133]. Compared to the commercial anthraquinone process for H_2O_2 production, the synthesis of H_2O_2 via photocatalytic oxygen reduction is a more environmentally friendly pathway[134]. To date, supramolecular materials, conjugated polymers, covalent organic frameworks, and g-C_3N_4-based materials have all shown their potential for

Table 1. State-of-the-art organic semiconductor photocatalysts in CO_2 reduction

Photocatalysts	Product	Reaction rate ($\mu mol \cdot g^{-1} \cdot h^{-1}$)	Illumination source	Reaction solvent	Reference
COF-367-Co NSs	CO	10,162	300 W Xe lamp, $\lambda \geq 420$ nm	$KHCO_3$ (aq)	[125]
Co-2,3-DHTA-COF	CO	18,000	300 W Xe lamp, $\lambda > 420$ nm	CH_3CN/H_2O	[126]
Ru-CTF-2	HCOOH	2,090	8W LED lamp	N,N-dimethylacetamide/TEOA	[127]
TpBD-$(OCH_3)_2$	HCOOH	108.3	300 W Xe lamp, 800 nm $\geq \lambda \geq$ 420 nm	CH_3CN/TEOA	[128]
TEB-PQ	CH_4	269	300 W Xe lamp, $\lambda > 420$ nm	CH_3CN/H_2O	[130]
TPA-PQ	CH_4	2,150	300 W Xe lamp, $\lambda > 420$ nm	CH_3CN/H_2O	[130]
PdIn@N3-COF	CH_3OH	24.5	300 W Xe lamp, $\lambda \geq 400$ nm	H_2O	[131]
PdIn@N3-COF	C_2H_5OH	8.75	300W Xe lamp, $\lambda \geq 400$ nm	H_2O	[131]
ON-MOP	C_2H_5OH	800	300 W Xe lamp, $\lambda > 420$ nm	$NaHCO_3$(aq)/K_2SO_3(aq)	[132]

photocatalytic H_2O_2 production[134-137]. The more efficient approach toward H_2O_2 production is the two-electron oxygen reduction pathway ($O_2 + 2e^- + 2H^+ = H_2O_2$, 0.695 V *vs.* NHE), as its oxidant potential of 0.695 V_{NHE} is much lower than that of two-electron water oxidation reaction ($2H_2O + 2h^+ = H_2O_2 + 2H^+$, 1.76 V *vs.* NHE)[138]. It is reported that adjacent nitrogen atoms in covalent organic frameworks can facilitate O_2 adsorption, leading to an enhanced activity in H_2O_2 generation via the two-electron oxygen reduction pathway[139]. Therefore, efforts have been made to explore nitrogen-rich organic semiconductor photocatalysts. Zhang *et al.* designed and synthesized the self-assembled porphyrin-derivative supramolecular catalysts that enabled H_2O_2 generation from H_2O and O_2. This photocatalyst achieved a quantum efficiency of 14.9% at 420 nm and a solar-to-chemical conversion efficiency of 1.2% under simulated sunlight illumination[140]. Remarkably, this high photocatalytic activity of H_2O_2 production was achieved without the assistance of sacrificial agents, which has inspired other researchers to explore non-sacrificial H_2O_2 generation using organic semiconductors[141].

In addition to hydrogen evolution, CO_2 reduction, and H_2O_2 production reactions, recent years have also seen the application of organic semiconductors in the photocatalytic degradation of pollutants and organic synthesis[142].

Shortcomings of organic semiconductor photocatalysts

Although organic semiconductors display their capability in solar fuel production and environmental remediation, some shortcomings of organic semiconductors still hinder the enhancement of their photocatalytic activity.

Large exciton binding energy

The exciton is a quasi-particle in semiconductors composed of an electron-hole pair bound together by the Coulomb interaction[143]. The energy separating the bounded electron-hole pair is called the exciton binding energy, which is affected by the strength of the Coulomb interaction[144-146]. When the size of an inorganic semiconductor goes down from bulk to subnanoscale, the Coulomb force in the exciton becomes significantly stronger. Specifically, both the monolayer of two-dimensional material and a quantum dot have a larger exciton binding energy than their bulk counterparts due to their stronger excitonic Coulomb interactions[144-146]. It is well known that the binding energy of exciton (E_b) is inversely correlated to the exciton Bohr radius a_0^* and dielectric constant (ε_r): $E_b = \frac{e^2}{\varepsilon_0 \varepsilon_r a_0^*}$ (e is the elementary charge)[147]. Hence, E_b will increase with the decrease of exciton Bohr radius in semiconductors. In general, excitons are classified into two different types - Frenkel exciton (a smaller exciton radius) and Wannier-Mott exciton (a larger exciton radius)[148]. Frenkel excitons often exist in organic semiconductors, where the electron-hole relative distance

is limited to one or only a few neighboring unit cells[148]. Consequently, organic semiconductors usually possess a smaller exciton Bohr radius. In contrast, the significant overlap of interatomic electronic wave functions in inorganic semiconductors allows electrons and holes to be bound over longer distances in the excitonic state. Therefore, exciton dissociation in organic semiconductors is more difficult than in inorganic semiconductors [Figure 5A and B], although tuning substituent groups and extending the conjugation length of the backbone can partially lower the exciton binding energy in organic semiconductors [Figure 5C and D][149]. In addition to the exciton Bohr radius, the relative dielectric constant ε_r is also inversely proportional to the exciton binding energy [Figure 5C]. Given that organic semiconductors typically have a much smaller ε_r than inorganic semiconductors[148], the exciton binding energy in organic semiconductors becomes significantly higher than that in their inorganic counterparts. As a result, a smaller exciton Bohr radius and a lower dielectric constant synergistically lead to an exciton binding energy that is one or two orders of magnitude greater in organic semiconductors compared to inorganic semiconductors.

Short exciton diffusion length and low charge carrier mobility

The exciton diffusion length and charge carrier mobility in organic semiconductors are crucial factors influencing photon-to-electron conversion efficiency[150]. Due to their electrical neutrality, excitons in semiconductors primarily move by diffusion rather than drift. The exciton diffusion length, defined as the average distance an exciton can travel before recombination, determines how many excitons reach the interface and thus affects electron-hole recombination. Generally, a longer exciton diffusion length allows more excitons in the bulk of organic semiconductors to reach the interface, thereby inhibiting the electron-hole radiative or non-radiative recombination[151]. However, the exciton diffusion length in organic semiconductors is typically less than 10 nm[152].

After exciton diffusion and dissociation, the generated electrons and holes migrate either in the bulk or toward the surface of photocatalysts. Unlike the band-like charge carrier transport in crystalline inorganic semiconductors, charge transport in organic semiconductors primarily occurs through inter-molecular hopping, where carriers move from one molecule to another[153-156]. This mode of transport results in significant charge carrier scattering, leading to a shorter mean free time and mean free path in organic semiconductors compared to inorganic semiconductors. According to the classical Drude model $\mu = \tau e/m^*$, the charge carrier mobility (μ) scales positively with the mean free time (τ) and is inversely proportional to the effective mass of the carrier (m^*). The shorter mean free time in organic semiconductors already reduces their mobility relative to inorganic semiconductors. Moreover, the effective masses of charge carriers in organic semiconductors are larger than those in inorganic semiconductors[157], further diminishing mobility. Consequently, the combination of shorter mean free times and larger effective masses results in charge carrier mobilities that are several orders of magnitude lower in organic semiconductors than in inorganic semiconductors under identical conditions. This intrinsic drawback tremendously limits the number of charge carriers that can reach the surface of organic semiconductors to trigger interfacial chemical reactions.

Chemical instability

The instability of organic semiconductors is a major disadvantage that hinders their practical application[158]. Although organic semiconductor solar cells are typically fabricated and assembled in an inert gas atmosphere with extremely low humidity[30], their practical application is still bottlenecked by issues related to device durability and lifespan[31]. Even when these devices are kept away from direct contact with inorganic or organic solvents, they still cannot maintain optimal performance for extended periods. This issue is even more pronounced for organic semiconductor photocatalysts, which are often tested in solvents or under harsher conditions, such as strong acids or alkaline environments. For example, boronate ester-

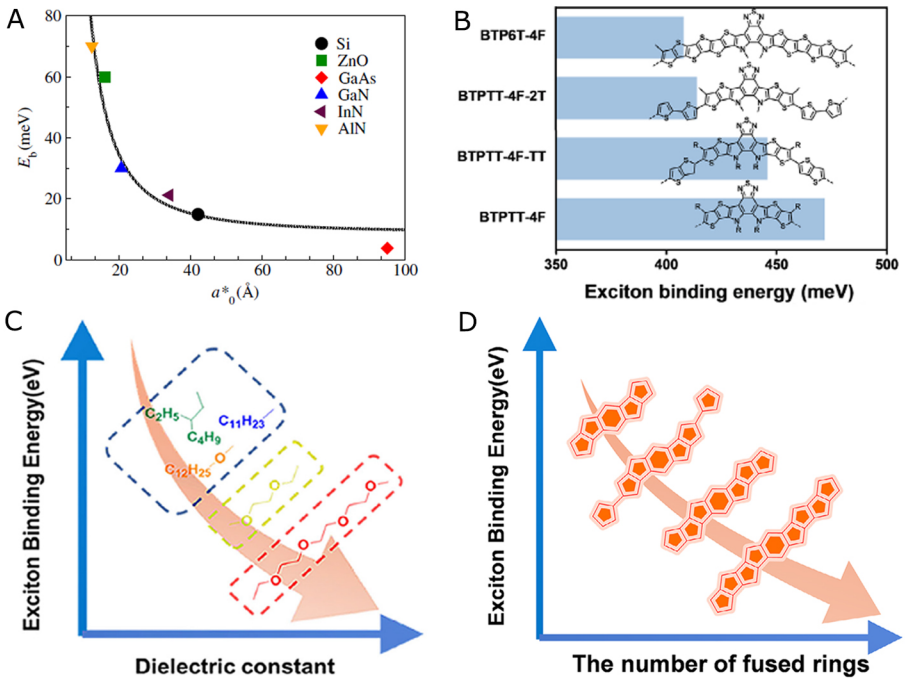

Figure 5. (A) Exciton binding energy in common inorganic semiconductors and its relationship with the exciton Bohr radius. Adapted with permission[147], Copyright 2013 American Physical Society; (B) Exciton binding energy in organic semiconductors; (C) Relationship between exciton binding energy and dielectric constant in organic semiconductors; (D) Exciton binding energy as a function of conjugation length in organic semiconductors[149], Copyright 2022 Wiley-VCH.

linked COFs decompose when exposed to water or moisture[159]. The photostability of organic semiconductor photocatalysts is another significant drawback. Different from the rigid and stable Ti-O octahedra building units in TiO_2[5], the C-N or C-O bonds in organic semiconductors are more prone to structural damage from surface-adsorbed hydroxyl radicals and photogenerated holes[160]. Graphitic carbon nitride (g-C_3N_4) has been extensively studied for solar water splitting and CO_2 reduction due to its suitable conduction band minimum potential and visible light response[62]. However, the origin of the CO_2 reduction products generated on g-C_3N_4 has not been traced in detail before. Chen *et al.* found that CO production occurs on g-C_3N_4 under light illumination, both in the presence and absence of a CO_2 gas atmosphere[160]. In other words, g-C_3N_4 undergoes rapid self-decomposition during the gas-solid photocatalytic CO_2 reduction process, accompanied by CO production. Specifically, hydroxyl groups attack the C–N=C structural units in g-C_3N_4, leading to the release of CO after a series of complex reactions. These findings highlight the possible structural damage to the backbones of ordinary organic semiconductors in photocatalysis, emphasizing the need to develop more robust organic semiconductor photocatalysts with improved chemical stability.

Solutions to the shortcomings of organic semiconductor photocatalysts

To overcome the shortcomings of organic semiconductors in photocatalysis, several strategies have been developed. π-conjugation extension is a feasible method to lower exciton binding energies in organic semiconductors. Donor-acceptor structure design and heterojunction can improve charge carrier dynamics. Modifying building blocks is also a viable strategy to extend exciton diffusion lengths and improve the chemical stability of organic semiconductors.

π-conjugation extension

After theoretically analyzing the electronic structures of 32 organic semiconductors, Sugie *et al.* identified a quasi-linear relationship between exciton binding energy and transport band gap, i.e., the exciton binding energy is one-quarter of the transport band gap[161]. It is well known that the band gaps of organic semiconductors decrease with the enlargement of π-conjugation. Accordingly, the exciton binding energy is also expected to decline with π-conjugation extension. Ma *et al.* directly proved this concept via theoretical calculations. They demonstrated that COFs formed by incorporating polyyne $(-C\equiv C-)_n$ groups between the tertiary amino group and the heptazine ring of the g-C_3N_4 skeleton show reduced exciton binding energies as the number of polyyne units increases[162]. Lan *et al.* further experimentally verified this strategy for lowering exciton binding energy in conjugated polymers. Using dibenzothiophene-S, S-dioxide (FSO) as an electron-deficient structural unit, they showed that replacing the electron-rich building block biphenyl (BP) with dibenzothiophene (FS) modulated the exciton binding energy in the resulting conjugated polymers[163]. The larger π-conjugation system in FS compared to BP endows the FSO-FS conjugated polymer with a lower exciton binding energy (88 meV) than that of FSO-BP (104 meV). This reduction in exciton binding energy in FSO-FS leads to a higher photocatalytic hydrogen evolution rate (170 μmol·h^{-1}) compared to FSO-BP (60 μmol·h^{-1})[163]. Thus, π-conjugation extension is both a theoretically and experimentally validated approach to reducing exciton binding energy in organic semiconductor photocatalysts.

Donor-acceptor structure design

The design of electron donor-acceptor (D-A) structures is a widely adopted strategy to facilitate exciton dissociation and charge carrier transport in organic semiconductor photocatalysts[164,165]. The difference in electron affinity between electron-rich donors and electron-deficient acceptors drives electron transfer from the donor to the acceptor in the excited state[166]. When electron donor and acceptor units coexist within the same molecule, an intramolecular D-A structure is formed, which can be realized in conjugated polymers and covalent organic frameworks [Figure 6A and B][166,167]. COFs featuring D-A designs have demonstrated exceptional capabilities in promoting exciton diffusion and charge delocalization, particularly in systems with fully π-conjugated skeletons and large crystalline domain sizes[168-172]. For example, coupling a π-conjugation electron donor system with a typical electron acceptor, such as benzothiadiazole, results in a D-A structure where photoexcited electrons accumulate at the benzothiadiazole unit. These electrons can then be transferred to protons through the catalytic sites provided by N heteroatoms in benzothiadiazole to generate H_2[173]. Utilizing benzothiadiazole as the electron acceptor unit, an imine-linked D-A-D structured COF has achieved a photocatalytic hydrogen evolution rate of 5,458 μmol·g^{-1}·h^{-1} under visible light illumination[174]. Moreover, built-in electric fields within intermolecular D-A-type structures can facilitate electron-hole separation [Figure 6C][175]. The dipole moment changes caused by these built-in electric fields accelerate exciton dissociation in supramolecular photocatalysts. For instance, tetraphenylporphinesulfonate (TPPS), an electron-donating building block with a large π-conjugated system, possesses a considerable dipole moment (3.94 D). Meanwhile, the well-known electron acceptor fullerene (C_{60}), with its highly delocalized π-electron surface, can bind to TPPS throughπ-π stacking interactions. The resulting TPPS-C_{60} hybrid forms a D-A supramolecular structure, leading to an enhanced electron polarization on TPPS and a significantly higher dipole moment (12.37 D). This 3.14-fold increase in dipole moment facilitates charge carrier separation and results in a 6.03-fold improvement in photocatalytic H_2 evolution rate compared to TPPS alone[175]. Additionally, tuning the distance between donor and acceptor units within the structure can further enhance photocatalytic activity[176]. For example, adjusting the σ-linkage length in the D-σ-A structure of imidazole-alkyl-perylene diimide enables optimization of the π-π stacking distance, a key factor influencing fast charge carrier transfer and reduced carrier recombination[177]. The supramolecular structure C2IPDI shows a shorter π-π stacking distance (3.19 Å) compared to C0IPDI (3.42 Å) and C3IPDI (3.33-3.51 Å)[176], resulting in the highest photocatalytic water oxidation activity among the three supramolecular photocatalysts.

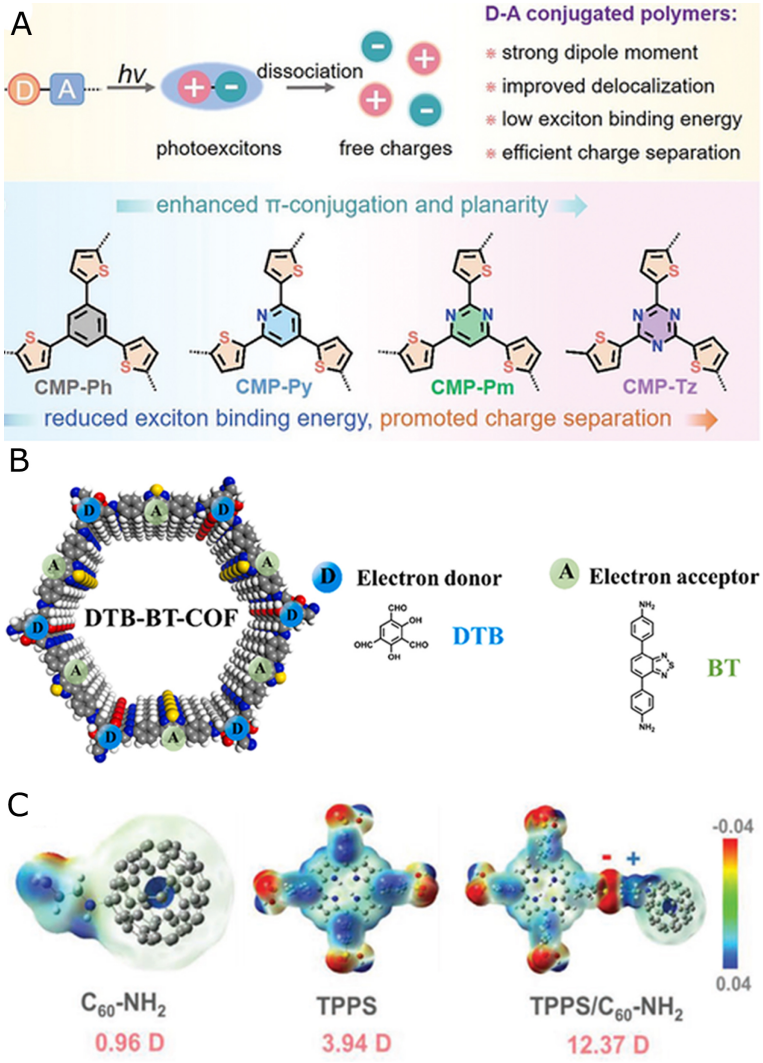

Figure 6. Design of Donor-Acceptor (D-A) structure in organic semiconductor photocatalysts: (A) Conjugated polymers with D-A structure. Adapted with permission[166], Copyright 2023 Wiley-VCH; (B) Covalent organic frameworks with D-A structure. Adapted with permission[167], Copyright 2022 Elsevier Ltd; (C) Supramolecular composites with D-A structure. Adapted with permission[175], Copyright 2021 Wiley-VCH.

Heterojunction

Constructing a heterojunction between two organic semiconductors is also a feasible way to promote photoexcited electron-hole separation and transport[178]. Similar to heterojunctions formed between two inorganic materials, proper band alignment is a prerequisite for the formation of organic semiconductor heterojunctions. The staggered CBM and VBM energy levels drive charge transfer between the two organic semiconductors - electrons are collected by the semiconductor with the lower CBM position, while holes accumulate in the semiconductor with the higher VBM position. Specifically, the donor polymer PTB7-Th can form a type II heterojunction with EH-IDTBR, where the staggered bandgap enables highly efficient electron-hole separation. As a result, the PTB7-Th/EH-IDTBR organic heterojunction exhibits significantly higher photocatalytic hydrogen evolution activity than benchmark photocatalysts such as TiO_2 and C_3N_4[179]. In addition to favorable band alignment, efficient sunlight harvesting is also essential for constructing effective heterojunctions. According to the U.S. Department of Energy's solar-driven photocatalytic hydrogen production guidelines, commercial application of solar-driven photocatalytic hydrogen

production is not feasible if a photocatalyst lacks activity at wavelengths above 500 nm[180]. In this scenario, an inorganic/organic S-scheme heterojunction was formed by growing CdS nanocrystals on the surface of a pyrene-based conjugated polymer[181]. Both the CdS nanocrystals and the pyrene-based polymer show absorption edges beyond 500 nm, thereby meeting the threshold for achieving high solar-to-chemical conversion efficiency. Furthermore, the staggered energy bands generate a built-in electric field that facilitates highly efficient hole-electron separation, resulting in a prominent apparent quantum efficiency of 24.3% under visible light irradiation[181]. Additionally, a ternary heterojunction composed of PM6, ICTT-M, and IDMIC-4F - organic semiconductors with strong absorption in the 600-800 nm wavelength range - achieved an apparent quantum yield of 5.9% at 600 nm. This further highlights the vital importance of heterojunctions with broad solar spectrum response in boosting exciton dissociation and charge carrier transport[182].

Building block modification

Modifying the building blocks (i.e., the backbones and substituent groups) of organic semiconductors can effectively extend the exciton diffusion length and improve charge carrier transport. For example, removing the electron-withdrawing thiadiazole units from the backbone of the photovoltaic material Y6 [Figure 7A] results in a new semiconductor molecule, F1, which exhibits an exciton diffusion length 1.67 times greater than that of Y6. This improvement further leads to a 2.26-fold increase in the photocatalytic H_2 evolution rate for F1 compared to Y6 under AM 1.5G light irradiation[151]. In addition to tuning the backbone structure, modifying substituent groups also improves charge carrier dynamics in organic semiconductor photocatalysts [Figure 7B]. For instance, the incorporation of a 4-carboxylphenyl group into a porphyrin molecule yields Tetra(4-carboxylphenyl)porphyrin, which possesses a molecular dipole moment of 4.08 Debye (D) - significantly higher than that of Tetra(4-cyanophenyl)porphyrin (0.14 D) and Tetra(4-pyridylphenyl)porphyrin (0.08 D). A higher dipole moment markedly enhances the photocatalytic water-splitting activity of Tetra(4-carboxylphenyl)porphyrin by promoting more efficient electron-hole separation[183]. Beyond improving exciton binding, electron-hole recombination, and charge carrier transport, modifying the building blocks also addresses the chemical instability of organic semiconductor photocatalysts. One effective strategy for enhancing chemical stability is increasing the hydrophobicity of the backbones. For example, the periodic incorporation of isopropyl groups imparts COFs with robust resistance to strong acids and bases[184], as the hydrophobicity of isopropyl groups protects the otherwise hydrolytically sensitive backbones of COFs[185]. To fundamentally overcome the chemical instability of COFs in photocatalysis, a general strategy involves replacing reversible linkages with irreversible ones during COF construction[186,187]. For instance, boronate ester linkages - formed through the condensation of a boronic acid and a diol, releasing two water molecules[159] - are reversible. Consequently, boronate ester-linked COFs can hydrolyze in the presence of water, regenerating the boronic acid and diol and leading to COF decomposition. To address this issue, using building units such as triazine, annulative, and quinoline enables the formation of irreversible linkages, substantially enhancing the chemical stability of COFs [Figure 7C].

CONCLUSION

As discussed above, organic semiconductors with large absorption coefficients, tuneable electronic band structures, and controllable dielectric constants have shown merits in boosting photocatalytic reactivity. However, drawbacks in exciton dissociation, exciton diffusion, charge carrier transport, and chemical stability still hinder their practical application in photocatalysis. In addition to well-established strategies for optimizing photocatalytic performance - such as π-conjugation extension, donor-acceptor structural design, interface engineering, and building block modification - the following aspects should also be considered to further improve exciton dissociation, exciton diffusion, surface catalytic activity, and chemical stability:

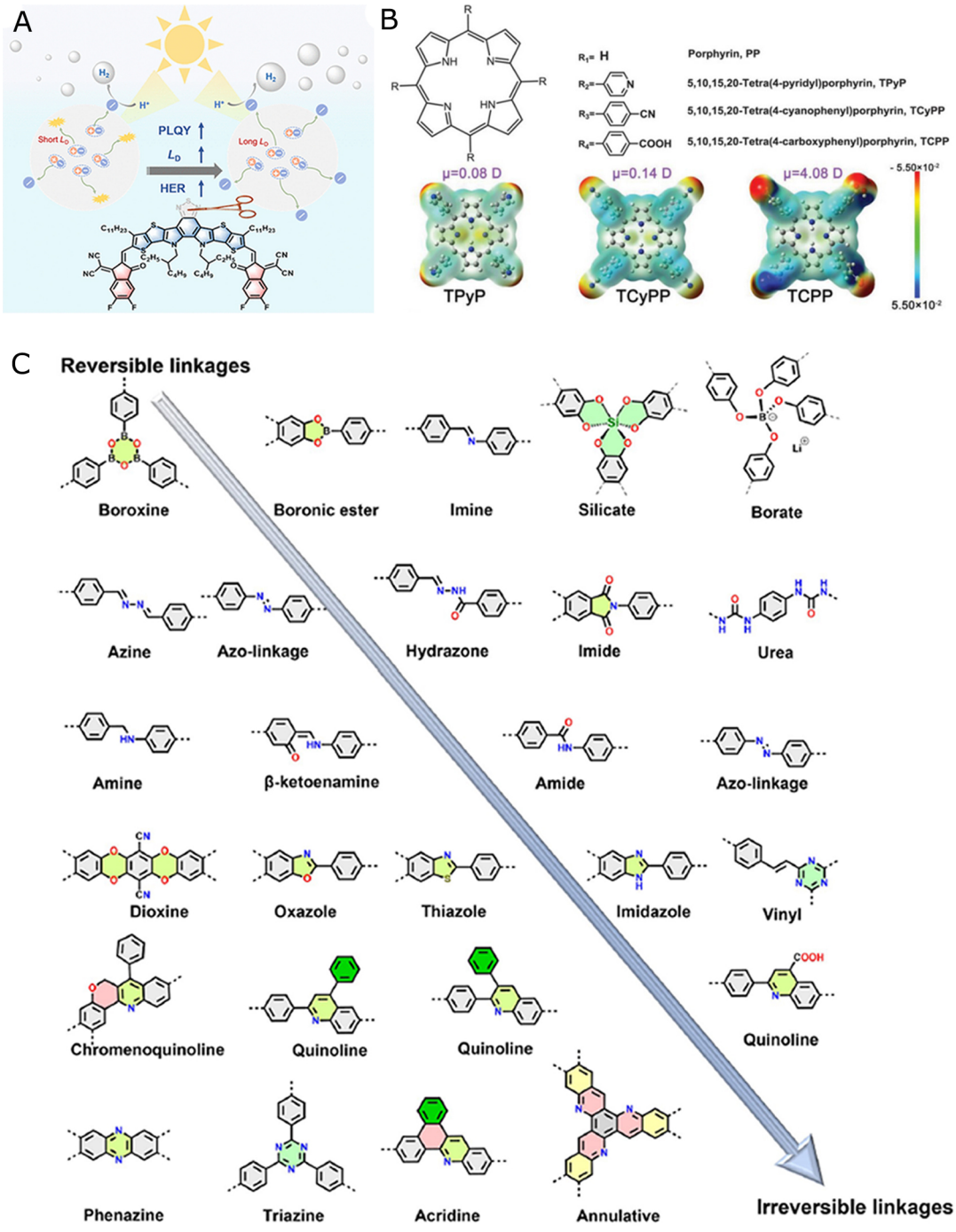

Figure 7. Modifying the building blocks of organic semiconductors to enhance charge carrier dynamics and chemical stability: (A) Tailoring the molecular backbone. Adapted with permission[151], Copyright 2022 American Chemical Society; (B) Modifying substituent groups. Adapted with permission[183], Copyright 2019 Wiley-VCH; (C) Introducing irreversible linkages to enhance the chemical stability of COFs[186], Copyright 2024 American Chemical Society.

Enhancing the Dielectric Constant: A high dielectric constant can not only reduce exciton binding energy but also suppress electron-hole recombination in organic semiconductors. Therefore, greater efforts are needed to design and synthesize organic semiconductor photocatalysts with elevated dielectric constants. One approach involves incorporating functional groups with flexible permanent dipoles into the molecular

structures of organic semiconductors[102]. For example, ethylene glycol (EG) chains, which possess permanent dipoles and maintain conformational flexibility in the solid state, can reorient rapidly and thereby help enhance the dielectric constant[102]. Additionally, the polarizability of the molecules significantly affects the dielectric constant. Incorporating non-fullerene building units with large fused-ring structures offers a promising route to increasing molecular polarizability and, consequently, the dielectric constant[188].

Optimizing Surface Catalysis in Porous Structures: Beyond light absorption, exciton dissociation, and charge carrier transport, surface catalysis plays a crucial role in improving photocatalytic performance. The catalytic sites in organic photocatalysts influence reactant adsorption, the efficiency of charge carrier transfer to adsorbed reactants, and product desorption. In porous organic photocatalysts, fine-tuning the chemical environment within pores and modifying the structure of pore walls are key strategies for enhancing photocatalytic efficiency[189-192]. Such designs can improve hydrophilicity and reactant accessibility. For instance, chiral pore environments can promote enantioselective reactions and facilitate product separation[193-195]. Moreover, rationally designed pore walls allow precise regulation of cocatalyst loading and distribution, which can lower the overpotential of specific reactions[18,99]. Pore size also significantly affects the photocatalyst's surface area and the mass transport of reactants and products, ultimately influencing turnover rates and overall catalytic efficiency[196-199]. Larger and more flexible pores generally improve molecular dynamics, enhancing reactant utilization and product release. Therefore, future research should focus on constructing large and adaptable pore structures in organic semiconductors.

Balancing Stability and Activity: In some cases, enhancing photocatalytic activity may compromise the stability of organic semiconductors. For example, increasing hydrophilicity can significantly enhance photocatalytic H_2 production[115,200], but the reversible linkage of hydrophilic building blocks may lead to the destruction of the semiconductor framework[159]. Therefore, achieving chemical stability without sacrificing catalytic activity is critical for designing robust organic semiconductor photocatalysts. In this context, employing irreversible linkages lays a solid foundation for enhancing long-term chemical stability. Furthermore, integrating hydrophilic building blocks with irreversible linkages, such as carboxyl-substituted quinoline or imidazole, could enable the construction of highly durable organic photocatalysts.

DECLARATIONS

Acknowledgments

This paper was supported by the Joint Usage/Research Center for Catalysis.

Authors' contributions

Conceptualization, Formal analysis, Project administration, Writing-original draft, Writing-review & editing: Lin, R.
Formal Analysis, Writing-review & editing: Hsueh, C.H.; Yu, H.
Resources support: Heine, T.; Chen, C.
Administrative support, Writing-review & editing: Murayama, T.

Availability of data and materials

Not applicable.

Financial support and sponsorship

None.

Conflicts of interest

All authors declared that there are no conflicts of interest.

Ethical approval and consent to participate

Not applicable.

Consent for publication

Not applicable.

REFERENCES

1. Fujishima, A.; Honda, K. Electrochemical photolysis of water at a semiconductor electrode. *Nature* **1972**, *238*, 37-8. DOI PubMed
2. Lang, X.; Chen, X.; Zhao, J. Heterogeneous visible light photocatalysis for selective organic transformations. *Chem. Soc. Rev.* **2014**, *43*, 473-86. DOI PubMed
3. Song, H.; Meng, X.; Wang, S.; et al. Direct and selective photocatalytic oxidation of CH_4 to oxygenates with O_2 on cocatalysts/ZnO at room temperature in water. *J. Am. Chem. Soc.* **2019**, *141*, 20507-15. DOI PubMed
4. Yoshino, S.; Takayama, T.; Yamaguchi, Y.; Iwase, A.; Kudo, A. CO_2 reduction using water as an electron donor over heterogeneous photocatalysts aiming at artificial photosynthesis. *Acc. Chem. Res.* **2022**, *55*, 966-77. DOI PubMed PMC
5. Guo, Q.; Zhou, C.; Ma, Z.; Yang, X. Fundamentals of TiO_2 photocatalysis: concepts, mechanisms, and challenges. *Adv. Mater.* **2019**, *31*, 1901997. DOI PubMed
6. Abe, R.; Higashi, M.; Domen, K. Facile fabrication of an efficient oxynitride TaON photoanode for overall water splitting into H_2 and O_2 under visible light irradiation. *J. Am. Chem. Soc.* **2010**, *132*, 11828-9. DOI PubMed
7. Zhao, L.; Hou, H.; Wang, S.; et al. Engineering Co single atoms in ultrathin BiOCl nanosheets for boosted CO_2 photoreduction. *Adv. Funct. Mater.* **2025**, *35*, 2416346. DOI
8. Zong, X.; Yan, H.; Wu, G.; et al. Enhancement of photocatalytic H_2 evolution on CdS by loading MoS_2 as Cocatalyst under visible light irradiation. *J. Am. Chem. Soc.* **2008**, *130*, 7176-7. DOI PubMed
9. Takanabe, K. Photocatalytic water splitting: quantitative approaches toward photocatalyst by design. *ACS Catal.* **2017**, *7*, 8006-22. DOI
10. Zhang, M.; Chen, C.; Ma, W.; Zhao, J. Visible-light-induced aerobic oxidation of alcohols in a coupled photocatalytic system of dye-sensitized TiO_2 and TEMPO. *Angew. Chem. Int. Ed.* **2008**, *47*, 9730-3. DOI PubMed
11. Wang, C.; Thompson, R. L.; Ohodnicki, P.; Baltrus, J.; Matranga, C. Size-dependent photocatalytic reduction of CO_2 with PbS quantum dot sensitized TiO_2 heterostructured photocatalysts. *J. Mater. Chem.* **2011**, *21*, 13452-7. DOI
12. Asahi, R.; Morikawa, T.; Ohwaki, T.; Aoki, K.; Taga, Y. Visible-light photocatalysis in nitrogen-doped titanium oxides. *Science* **2001**, *293*, 269-71. DOI PubMed
13. Jiang, Y.; Sun, H.; Guo, J.; et al. Vacancy engineering in 2D transition metal chalcogenide photocatalyst: structure modulation, function and synergy application. *Small* **2024**, *20*, 2310396. DOI PubMed
14. Niu, M.; Huang, F.; Cui, L.; Huang, P.; Yu, Y.; Wang, Y. Hydrothermal synthesis, structural characteristics, and enhanced photocatalysis of SnO_2/alpha-Fe_2O_3 semiconductor nanoheterostructures. *ACS Nano* **2010**, *4*, 681-8. DOI PubMed
15. Shi, R.; Zhao, Y.; Waterhouse, G. I. N.; Zhang, S.; Zhang, T. Defect engineering in photocatalytic nitrogen fixation. *ACS Catal.* **2019**, *9*, 9739-50. DOI
16. Lin, R.; Wan, J.; Xiong, Y.; et al. Quantitative study of charge carrier dynamics in well-defined WO_3 nanowires and nanosheets: insight into the crystal facet effect in photocatalysis. *J. Am. Chem. Soc.* **2018**, *140*, 9078-82. DOI PubMed
17. Lin, R.; Chen, H.; Cui, T.; et al. Optimization of p-type Cu_2O nanocube photocatalysts based on electronic effects. *ACS Catal.* **2023**, *13*, 11352-61. DOI
18. Ran, J.; Jaroniec, M.; Qiao, S. Z. Cocatalysts in semiconductor-based photocatalytic CO_2 reduction: achievements, challenges, and opportunities. *Adv. Mater.* **2018**, *30*, 1704649. DOI PubMed
19. Ou, W.; Zhou, B.; Shen, J.; Zhao, C.; Li, Y. Y.; Lu, J. Plasmonic metal nanostructures: concepts, challenges and opportunities in photo-mediated chemical transformations. *iScience* **2021**, *24*, 101982. DOI PubMed PMC
20. Zhou, L.; Huang, Q.; Xia, Y. Plasmon-induced hot electrons in nanostructured materials: generation, collection, and application to photochemistry. *Chem. Rev.* **2024**, *124*, 8597-619. DOI PubMed PMC
21. Lin, R.; Fan, D.; Berger, L. M.; et al. Light tuning CO/H_2 composition on Ag: unraveling CO_2 mass transfer and electron-phonon coupling in plasmon-enhanced electrocatalysis. *Nano Res.* **2025**, *18*, 94907042. DOI
22. Fu, Y.; Sun, D.; Chen, Y.; et al. An amine-functionalized titanium metal-organic framework photocatalyst with visible-light-induced activity for CO_2 reduction. *Angew. Chem. Int. Ed.* **2012**, *51*, 3364-7. DOI PubMed

23. Navalón, S.; Dhakshinamoorthy, A.; Álvaro, M.; Ferrer, B.; García, H. Metal-organic frameworks as photocatalysts for solar-driven overall water splitting. *Chem. Rev.* **2023**, *123*, 445-90. DOI PubMed PMC
24. Wang, Q.; Gao, Q.; Al-Enizi, A. M.; Nafady, A.; Ma, S. Recent advances in MOF-based photocatalysis: environmental remediation under visible light. *Inorg. Chem. Front.* **2020**, *7*, 300-39. DOI
25. Silva, C. G.; Corma, A.; García, H. Metal-organic frameworks as semiconductors. *J. Mater. Chem.* **2010**, *20*, 3141-56. DOI
26. Alvaro, M.; Carbonell, E.; Ferrer, B.; Llabrés i Xamena, F. X.; Garcia, H. Semiconductor behavior of a metal-organic framework (MOF). *Chem. Eur. J.* **2007**, *13*, 5106-12. DOI PubMed
27. Kippelen, B.; Brédas, J. L. Organic photovoltaics. *Energy Environ. Sci.* **2009**, *2*, 251-61. DOI
28. Ma, Z.; Zhao, B.; Gao, H.; Gong, Y.; Yu, R.; Tan, Z. Recent advances of crosslinkable organic semiconductors in achieving solution-processed and stable optoelectronic devices. *J. Mater. Chem. A* **2022**, *10*, 18542-76. DOI
29. Jagoo, Z.; Lamport, Z. A.; Jurchescu, O. D.; McNeil, L. E. Efficiency enhancement of organic thin-film phototransistors due to photoassisted charge injection. *Appl. Phys. Lett.* **2021**, *119*, 073302. DOI
30. Fu, J.; Fong, P. W. K.; Liu, H.; et al. 19.31% binary organic solar cell and low non-radiative recombination enabled by non-monotonic intermediate state transition. *Nat. Commun.* **2023**, *14*, 1760. DOI PubMed PMC
31. Chen, L. X. Organic solar cells: recent progress and challenges. *ACS Energy Lett.* **2019**, *4*, 2537-9. DOI
32. Brütting, W. *Physics of Organic Semiconductors*; Wiley-VCH Verlag GmbH & Co. KGaA, 2005. DOI
33. Kuramochi, Y.; Fujisawa, Y.; Satake, A. Photocatalytic CO_2 reduction mediated by electron transfer via the excited triplet state of Zn(II) porphyrin. *J. Am. Chem. Soc.* **2020**, *142*, 705-9. DOI PubMed
34. Li, L.; Lo, W. Y.; Cai, Z.; Zhang, N.; Yu, L. Donor-acceptor porous conjugated polymers for photocatalytic hydrogen production: the importance of acceptor comonomer. *Macromolecules* **2016**, *49*, 6903-9. DOI
35. Ong, W. J.; Tan, L. L.; Ng, Y. H.; Yong, S. T.; Chai, S. P. Graphitic carbon nitride (g-C_3N_4)-based photocatalysts for artificial photosynthesis and environmental remediation: are we a step closer to achieving sustainability? *Chem. Rev.* **2016**, *116*, 7159-329. DOI PubMed
36. Ding, S. Y.; Wang, W. Covalent organic frameworks (COFs): from design to applications. *Chem. Soc. Rev.* **2013**, *42*, 548-68. DOI PubMed
37. Huang, F.; Anslyn, E. V. Introduction: supramolecular chemistry. *Chem. Rev.* **2015**, *115*, 6999-7000. DOI PubMed
38. Vallavoju, N.; Sivaguru, J. Supramolecular photocatalysis: combining confinement and non-covalent interactions to control light initiated reactions. *Chem. Soc. Rev.* **2014**, *43*, 4084-101. DOI PubMed
39. Dumele, O.; Chen, J.; Passarelli, J. V.; Stupp, S. I. Supramolecular energy materials. *Adv. Mater.* **2020**, *32*, 1907247. DOI PubMed
40. Nikoloudakis, E.; López-Duarte, I.; Charalambidis, G.; Ladomenou, K.; Ince, M.; Coutsolelos, A. G. Porphyrins and phthalocyanines as biomimetic tools for photocatalytic H_2 production and CO_2 reduction. *Chem. Soc. Rev.* **2022**, *51*, 6965-7045. DOI PubMed
41. Lopes, J. M. S.; Batista, A. A.; Araujo, P. T.; Neto, N. M. B. Supramolecular porphyrin as an improved photocatalyst for chloroform decomposition. *RSC Adv.* **2023**, *13*, 5473-82. DOI PubMed PMC
42. Würthner, F. Perylene bisimide dyes as versatile building blocks for functional supramolecular architectures. *Chem. Commun.* **2004**, *40*, 1564-79. DOI PubMed
43. Sun, Y.; Wang, D.; Zhu, Y. Deep degradation of pollutants by perylene diimide supramolecular photocatalyst with unique Bi-planar π-π conjugation. *Chem. Eng. J.* **2022**, *438*, 135667. DOI
44. Kong, K.; Zhang, S.; Chu, Y.; et al. A self-assembled perylene diimide nanobelt for efficient visible-light-driven photocatalytic H_2 evolution. *Chem. Commun.* **2019**, *55*, 8090-3. DOI PubMed
45. Li, Y.; Zhang, X.; Liu, D. Recent developments of perylene diimide (PDI) supramolecular photocatalysts: a review. *J. Photoch. Photobio. C* **2021**, *48*, 100436. DOI
46. Tamaki, Y.; Ishitani, O. Supramolecular photocatalysts for the reduction of CO_2. *ACS Catal.* **2017**, *7*, 3394-409. DOI
47. O'Neill, J. S.; Kearney, L.; Brandon, M. P.; Pryce, M. T. Design components of porphyrin-based photocatalytic hydrogen evolution systems: a review. *Coord. Chem. Rev.* **2022**, *467*, 214599. DOI
48. Wang, J.; Zhong, Y.; Wang, L.; et al. Morphology-controlled synthesis and metalation of porphyrin nanoparticles with enhanced photocatalytic performance. *Nano Lett.* **2016**, *16*, 6523-8. DOI PubMed
49. Zhang, N.; Wang, L.; Wang, H.; et al. Self-assembled one-dimensional porphyrin nanostructures with enhanced photocatalytic hydrogen generation. *Nano Lett.* **2018**, *18*, 560-6. DOI PubMed
50. Moon, H. S.; Yong, K. Noble-metal free photocatalytic hydrogen generation of CuPc/TiO_2 nanoparticles under visible-light irradiation. *Appl. Surf. Sci.* **2020**, *530*, 147215. DOI
51. Genc, E.; Yüzer, A. C.; Yanalak, G.; et al. The effect of central metal in phthalocyanine for photocatalytic hydrogen evolution via artificial photosynthesis. *Renew. Energy* **2020**, *162*, 1340-6. DOI
52. Han, J.; Liu, K.; Chang, R.; Zhao, L.; Yan, X. Photooxidase-mimicking nanovesicles with superior photocatalytic activity and stability based on amphiphilic amino acid and phthalocyanine co-assembly. *Angew. Chem. Int. Ed.* **2019**, *58*, 2000-4. DOI PubMed
53. Müllen, K.; Scherf, U. Conjugated polymers: where we come from, where we stand, and where we might go. *Macromol. Chem. Phys.* **2023**, *224*, 2200337. DOI
54. Banerjee, T.; Podjaski, F.; Kröger, J.; Biswal, B. P.; Lotsch, B. V. Polymer photocatalysts for solar-to-chemical energy conversion. *Nat. Rev. Mater.* **2021**, *6*, 168-90. DOI
55. Yanagida, S.; Kabumoto, A.; Mizumoto, K.; Pac, C.; Yoshino, K. Poly(p-phenylene)-catalysed photoreduction of water to hydrogen.

J. Chem. Soc. Chem. Commun. **1985**, *8*, 474-5. DOI
56. Sprick, R. S.; Aitchison, C.M.; Berardo, E.; et al. Maximising the hydrogen evolution activity in organic photocatalysts by co-polymerisation. *J. Mater. Chem. A* **2018**, *6*, 11994-2003. DOI
57. Chang, C. L.; Lin, W. C.; Ting, L. Y.; et al. Main-chain engineering of polymer photocatalysts with hydrophilic non-conjugated segments for visible-light-driven hydrogen evolution. *Nat. Commun.* **2022**, *13*, 5460. DOI PubMed PMC
58. Diao, R.; Ye, H.; Yang, Z.; Zhang, S.; Kong, K.; Hua, J. Significant improvement of photocatalytic hydrogen evolution of diketopyrrolopyrrole-based donor-acceptor conjugated polymers through side-chain engineering. *Polym. Chem.* **2019**, *10*, 6473-80. DOI
59. Hu, Z.; Wang, Z.; Zhang, X.; et al. Conjugated polymers with oligoethylene glycol side chains for improved photocatalytic hydrogen evolution. *iScience* **2019**, *13*, 33-42. DOI PubMed PMC
60. Lyons, R. J.; Yang, Y.; McQueen, E.; et al. Polymer photocatalysts with side chain induced planarity for increased activity for sacrificial hydrogen production from water. *Adv. Energy Mater.* **2024**, *14*, 2303680. DOI
61. Anus, A.; Park, S. The synthesis and key features of 3D carbon nitrides (C_3N_4) used for CO_2 photoreduction. *Chem. Eng. J.* **2024**, *486*, 150213. DOI
62. Chu, S.; Wang, Y.; Guo, Y.; et al. Band structure engineering of carbon nitride: in search of a polymer photocatalyst with high photooxidation property. *ACS Catal.* **2013**, *3*, 912-9. DOI
63. Wang, X.; Maeda, K.; Thomas, A.; et al. A metal-free polymeric photocatalyst for hydrogen production from water under visible light. *Nat. Mater.* **2009**, *8*, 76-80. DOI PubMed
64. Ding, Z.; Chen, X.; Antonietti, M.; Wang, X. Synthesis of transition metal-modified carbon nitride polymers for selective hydrocarbon oxidation. *ChemSusChem* **2011**, *4*, 274-81. DOI PubMed
65. Harikrishnan, L.; Rajaram, M.; Natarajan, A.; Rajaram, A. Boron-doped exfoliated g-C_3N_4 nanosheet-based phosphors for white light-emission and photocatalytic degradation. *ACS Appl. Nano Mater.* **2023**, *6*, 16947-59. DOI
66. Liu, G.; Niu, P.; Sun, C.; et al. Unique electronic structure induced high photoreactivity of sulfur-doped graphitic C_3N_4. *J. Am. Chem. Soc.* **2010**, *132*, 11642-8. DOI PubMed
67. Zhu, Y. P.; Ren, T. Z.; Yuan, Z. Y. Mesoporous phosphorus-doped g-C_3N_4 nanostructured flowers with superior photocatalytic hydrogen evolution performance. *ACS Appl. Mater. Interfaces* **2015**, *7*, 16850-6. DOI PubMed
68. Naveed, A. B.; Javaid, A.; Zia, A.; et al. TiO_2/g-C_3N_4 binary composite as an efficient photocatalyst for biodiesel production from jatropha oil and dye degradation. *ACS Omega* **2023**, *8*, 2173-82. DOI PubMed PMC
69. Côté, A. P.; Benin, A. I.; Ockwig, N. W.; O'Keeffe, M.; Matzger, A. J.; Yaghi, O. M. Porous, crystalline, covalent organic frameworks. *Science* **2005**, *310*, 1166-70. DOI PubMed
70. Waller, P. J.; Gándara, F.; Yaghi, O. M. Chemistry of covalent organic frameworks. *Acc. Chem. Res.* **2015**, *48*, 3053-63. DOI PubMed
71. Prakash, K.; Deka, R.; Mobin, S. M. A review on covalent organic frameworks: exploration of their growing potential as porous materials in photocatalytic applications. *Inorg. Chem. Front.* **2024**, *11*, 6711-52. DOI
72. Haase, F.; Lotsch, B. V. Solving the COF trilemma: towards crystalline, stable and functional covalent organic frameworks. *Chem. Soc. Rev.* **2020**, *49*, 8469-500. DOI PubMed
73. Yin, Y.; Zhang, Y.; Zhou, X.; et al. Ultrahigh-surface area covalent organic frameworks for methane adsorption. *Science* **2024**, *386*, 693-6. DOI PubMed
74. Wan, S.; Gándara, F.; Asano, A.; et al. Covalent organic frameworks with high charge carrier mobility. *Chem. Mater.* **2011**, *23*, 4094-7. DOI
75. Chen, Y.; Jiang, D. Photocatalysis with covalent organic frameworks. *Acc. Chem. Res.* **2024**, *57*, 3182-93. DOI PubMed
76. Yang, Q.; Luo, M.; Liu, K.; Cao, H.; Yan, H. Covalent organic frameworks for photocatalytic applications. *Appl. Catal. B: Environ.* **2020**, *276*, 119174. DOI
77. Yang, J.; Chen, Z.; Zhang, L.; Zhang, Q. Covalent organic frameworks for photocatalytic reduction of carbon dioxide: a review. *ACS Nano* **2024**, *18*, 21804-35. DOI PubMed
78. Wang, H.; Wang, H.; Wang, Z.; et al. Covalent organic framework photocatalysts: structures and applications. *Chem. Soc. Rev.* **2020**, *49*, 4135-65. DOI PubMed
79. Stegbauer, L.; Schwinghammer, K.; Lotsch, B. V. A hydrazone-based covalent organic framework for photocatalytic hydrogen production. *Chem. Sci.* **2014**, *5*, 2789-93. DOI
80. Gunawan, M.; Zhou, S.; Gunawan, D.; et al. Ferroelectric materials as photoelectrocatalysts: photoelectrode design rationale and strategies. *J. Mater. Chem. A* **2025**, *13*, 1612-40. DOI
81. Yao, L.; Rahmanudin, A.; Guijarro, N.; Sivula, K. Organic semiconductor based devices for solar water splitting. *Adv. Energy Mater.* **2018**, *8*, 1802585. DOI
82. McEvoy, A.; Markvart, T.; Castaner, L. *Practical Handbook of Photovoltaics: Fundamentals and Applications*, 2nd ed.; Academic Press, **2012**. DOI
83. Maeda, K.; Takata, T.; Hara, M.; et al. GaN:ZnO solid solution as a photocatalyst for visible-light-driven overall water splitting. *J. Am. Chem. Soc.* **2005**, *127*, 8286-7. DOI PubMed
84. Bronstein, H.; Nielsen, C. B.; Schroeder, B. C.; McCulloch, I. The role of chemical design in the performance of organic semiconductors. *Nat. Rev. Chem.* **2020**, *4*, 66-77. DOI PubMed

85. Wang, S. J.; Hutsch, S.; Talnack, F.; et al. Band structure engineering in highly crystalline organic semiconductors. *Chem. Mater.* **2023**, *35*, 7867-74. DOI
86. Ortstein, K.; Hutsch, S.; Hambsch, M.; et al. Band gap engineering in blended organic semiconductor films based on dielectric interactions. *Nat. Mater.* **2021**, *20*, 1407-13. DOI PubMed
87. Wang, Y.; Silveri, F.; Bayazit, M. K.; et al. Bandgap engineering of organic semiconductors for highly efficient photocatalytic water splitting. *Adv. Energy Mater.* **2018**, *8*, 1801084. DOI
88. Yu, H.; Wang, D. Suppressing the excitonic effect in covalent organic frameworks for metal-free hydrogen generation. *JACS Au* **2022**, *2*, 1848-56. DOI PubMed PMC
89. Van der Holst, J. J. M.; Van Oost, F. W. A.; Coehoorn, R.; Bobbert, P. A. Electron-hole recombination in disordered organic semiconductors: validity of the Langevin formula. *Phys. Rev. B* **2009**, *80*, 235202. DOI
90. Grinolds, D. D. W.; Brown, P. R.; Harris, D. K.; Bulovic, V.; Bawendi, M. G. Quantum-dot size and thin-film dielectric constant: precision measurement and disparity with simple models. *Nano Lett.* **2015**, *15*, 21-6. DOI PubMed
91. Wang, C.; Zhang, Z.; Pejić, S.; et al. High dielectric constant semiconducting poly(3-alkylthiophene)s from side chain modification with polar sulfinyl and sulfonyl groups. *Macromolecules* **2018**, *51*, 9368-81. DOI
92. Armin, A.; Stoltzfus, D. M.; Donaghey, J. E.; et al. Engineering dielectric constants in organic semiconductors. *J. Mater. Chem. C* **2017**, *5*, 3736-47. DOI
93. La, D. D.; Dang, T. D.; Le, P. C.; et al. Self-assembly of monomeric porphyrin molecules into nanostructures: self-assembly pathways and applications for sensing and environmental treatment. *Environ. Technol. Innov.* **2023**, *29*, 103019. DOI
94. Wang, Z.; Li, Z.; Medforth, C. J.; Shelnutt, J. A. Self-assembly and self-metallization of porphyrin nanosheets. *J. Am. Chem. Soc.* **2007**, *129*, 2440-1. DOI PubMed
95. Wang, Z.; Medforth, C. J.; Shelnutt, J. A. Porphyrin nanotubes by ionic self-assembly. *J. Am. Chem. Soc.* **2004**, *126*, 15954-5. DOI PubMed
96. Lee, J. S. M.; Cooper, A. I. Advances in conjugated microporous polymers. *Chem. Rev.* **2020**, *120*, 2171-214. DOI PubMed PMC
97. Liu, L.; Kochman, M. A.; Xu, Y.; Zwijnenburg, M. A.; Cooper, A. I.; Sprick, R. S. Acetylene-linked conjugated polymers for sacrificial photocatalytic hydrogen evolution from water. *J. Mater. Chem. A* **2021**, *9*, 17242-8. DOI
98. Geng, K.; He, T.; Liu, R.; et al. Covalent organic frameworks: design, synthesis, and functions. *Chem. Rev.* **2020**, *120*, 8814-933. DOI PubMed
99. Gong, Y. N.; Guan, X.; Jiang, H. L. Covalent organic frameworks for photocatalysis: synthesis, structural features, fundamentals and performance. *Coord. Chem. Rev.* **2023**, *475*, 214889. DOI
100. Huang, H.; Jiang, L.; Yang, J.; et al. Synthesis and modification of ultrathin g-C_3N_4 for photocatalytic energy and environmental applications. *Renew. Sustain. Energy Rev.* **2023**, *173*, 113110. DOI
101. Cao, S.; Low, J.; Yu, J.; Jaroniec, M. Polymeric photocatalysts based on graphitic carbon nitride. *Adv. Mater.* **2015**, *27*, 2150-76. DOI PubMed
102. Rousseva, S. Organic semiconductors with increased dielectric constants. Ph.D. Dissertation, University of Groningen, Groningen, Netherlands, 2022. https://doi.org/10.33612/diss.254084459 (assessed 2025-05-20)
103. Bertrandie, J.; Han, J.; De Castro, C. S. P.; et al. The energy level conundrum of organic semiconductors in solar cells. *Adv. Mater.* **2022**, *34*, 2202575. DOI
104. Hughes, M. P.; Rosenthal, K. D.; Ran, N. A.; Seifrid, M.; Bazan, G. C.; Nguyen, T. Q. Determining the dielectric constants of organic photovoltaic materials using impedance spectroscopy. *Adv. Funct. Mater.* **2018**, *28*, 1801542. DOI
105. Zhu, L.; Zhang, J.; Guo, Y.; Yang, C.; Yi, Y.; Wei, Z. Small exciton binding energies enabling direct charge photogeneration towards low-driving-force organic solar cells. *Angew. Chem. Int. Ed.* **2021**, *60*, 15348-53. DOI PubMed
106. Liu, X.; Yan, Y.; Honarfar, A.; Yao, Y.; Zheng, K.; Liang, Z. Unveiling excitonic dynamics in high-efficiency nonfullerene organic solar cells to direct morphological optimization for suppressing charge recombination. *Adv. Sci.* **2019**, *6*, 1802103. DOI PubMed PMC
107. de Clercq, D. M.; Yang, J.; Hanif, M.; et al. Exciton dissociation, charge transfer, and exciton trapping at the MoS_2/organic semiconductor interface. *J. Phys. Chem. C* **2023**, *127*, 11260-7. DOI
108. Sneyd, A. J.; Fukui, T.; Paleček, D.; et al. Efficient energy transport in an organic semiconductor mediated by transient exciton delocalization. *Sci. Adv.* **2021**, *7*, eabh4232. DOI PubMed PMC
109. Brédas, J. L.; Beljonne, D.; Coropceanu, V.; Cornil, J. Charge-transfer and energy-transfer processes in pi-conjugated oligomers and polymers: a molecular picture. *Chem. Rev.* **2004**, *104*, 4971-5004. DOI PubMed
110. Ma, D.; Zhang, Z.; Zou, Y.; Chen, J.; Shi, J. W. The progress of g-C_3N_4 in photocatalytic H_2 evolution: from fabrication to modification. *Coord. Chem. Rev.* **2024**, *500*, 215489. DOI
111. Jiang, J.; Cao, S.; Hu, C.; Chen, C. A comparison study of alkali metal-doped g-C_3N_4 for visible-light photocatalytic hydrogen evolution. *Chin. J. Catal.* **2017**, *38*, 1981-9. DOI
112. Zhang, J.; Zhang, M.; Sun, R. Q.; Wang, X. A facile band alignment of polymeric carbon nitride semiconductors to construct isotype heterojunctions. *Angew. Chem. Int. Ed.* **2012**, *51*, 10145-9. DOI PubMed
113. Hou, Y.; Laursen, A. B.; Zhang, J.; et al. Layered nanojunctions for hydrogen-evolution catalysis. *Angew. Chem. Int. Ed.* **2013**, *52*, 3621-5. DOI PubMed
114. He, F.; Chen, G.; Zhou, Y.; Yu, Y.; Zheng, Y.; Hao, S. The facile synthesis of mesoporous g-C_3N_4 with highly enhanced

photocatalytic H_2 evolution performance. *Chem. Commun.* **2015**, *51*, 16244-6. DOI PubMed

115. Wang, X.; Chen, L.; Chong, S. Y.; et al. Sulfone-containing covalent organic frameworks for photocatalytic hydrogen evolution from water. *Nat. Chem.* **2018**, *10*, 1180-9. DOI PubMed
116. Kosco, J.; Moruzzi, F.; Willner, B.; Mcculloch, I. Photocatalysts based on organic semiconductors with tunable energy levels for solar fuel applications. *Adv. Energy Mater.* **2020**, *10*, 2001935. DOI
117. Kosco, J.; Sachs, M.; Godin, R.; et al. The effect of residual palladium catalyst contamination on the photocatalytic hydrogen evolution activity of conjugated polymers. *Adv. Energy Mater.* **2018**, *8*, 1802181. DOI
118. Sachs, M.; Cha, H.; Kosco, J.; et al. Tracking charge transfer to residual metal clusters in conjugated polymers for photocatalytic hydrogen evolution. *J. Am. Chem. Soc.* **2020**, *142*, 14574-87. DOI PubMed PMC
119. Wang, Y.; Vogel, A.; Sachs, M.; et al. Current understanding and challenges of solar-driven hydrogen generation using polymeric photocatalysts. *Nat. Energy* **2019**, *4*, 746-60. DOI
120. Luo, T.; Gilmanova, L.; Kaskel, S. Advances of MOFs and COFs for photocatalytic CO_2 reduction, H_2 evolution and organic redox transformations. *Coord. Chem. Rev.* **2023**, *490*, 215210. DOI
121. Yeo, C. I.; Tan, Y. S.; Awan, H. T. A.; et al. A review on the advancements in covalent organic frameworks for photocatalytic reduction of carbon dioxide. *Coord. Chem. Rev.* **2024**, *521*, 216167. DOI
122. Fu, Y.; Zhu, X.; Huang, L.; Zhang, X.; Zhang, F.; Zhu, W. Azine-based covalent organic frameworks as metal-free visible light photocatalysts for CO_2 reduction with H_2O. *Appl. Catal. B: Environ.* **2018**, *239*, 46-51. DOI
123. Ai, L.; Li, W.; Wang, Q.; Cui, F.; Jiang, G. Harnessing keto-enol tautomerism to modulate β-ketoenamine-based covalent organic frameworks for visible-light-driven CO_2 reduction. *ChemCatChem* **2022**, *14*, e202200935. DOI
124. Yu, X.; Gong, K.; Tian, S.; Gao, G.; Xie, J.; Jin, X. H. A hydrophilic fully conjugated covalent organic framework for photocatalytic CO_2 reduction to CO nearly 100% using pure water. *J. Mater. Chem. A* **2023**, *11*, 5627-35. DOI
125. Liu, W.; Li, X.; Wang, C.; et al. A scalable general synthetic approach toward ultrathin imine-linked two-dimensional covalent organic framework nanosheets for photocatalytic CO_2 reduction. *J. Am. Chem. Soc.* **2019**, *141*, 17431-40. DOI PubMed
126. Zhang, Q.; Gao, S.; Guo, Y.; et al. Designing covalent organic frameworks with Co-O_4 atomic sites for efficient CO_2 photoreduction. *Nat. Commun.* **2023**, *14*, 1147. DOI PubMed PMC
127. Wang, L.; Wang, L.; Yuan, S.; et al. Covalently-bonded single-site Ru-N_2 knitted into covalent triazine frameworks for boosting photocatalytic CO_2 reduction. *Appl. Catal. B: Environ.* **2023**, *322*, 122097. DOI
128. Peng, L.; Chang, S.; Liu, Z.; et al. Visible-light-driven photocatalytic CO_2 reduction over ketoenamine-based covalent organic frameworks: role of the host functional groups. *Catal. Sci. Technol.* **2021**, *11*, 1717-24. DOI
129. Ferree, M.; Kosco, J.; Alshehri, N.; et al. Organic semiconductor nanoparticles for visible-light-driven CO_2 conversion. *Sustain. Energy Fuels* **2024**, *8*, 2423-30. DOI
130. Barman, S.; Singh, A.; Rahimi, F. A.; Maji, T. K. Metal-free catalysis: a redox-active donor-acceptor conjugated microporous polymer for selective visible-light-driven CO_2 reduction to CH_4. *J. Am. Chem. Soc.* **2021**, *143*, 16284-92. DOI PubMed
131. Huang, Y.; Du, P.; Shi, W. X.; et al. Filling COFs with bimetallic nanoclusters for CO_2-to-alcohols conversion with H_2O oxidation. *Appl. Catal. B: Environ.* **2021**, *288*, 120001. DOI
132. Tan, H.; Si, W.; Zhang, R.; et al. Dual active sites with charge-asymmetry in organic semiconductors promoting C-C coupling for highly efficient CO_2 photoreduction to ethanol. *Angew. Chem. Int. Ed.* **2025**, *64*, e202416684. DOI PubMed
133. Ciriminna, R.; Albanese, L.; Meneguzzo, F.; Pagliaro, M. Hydrogen peroxide: a key chemical for today's sustainable development. *ChemSusChem* **2016**, *9*, 3374-81. DOI PubMed
134. Li, W.; Han, B.; Liu, Y.; et al. Unsymmetric protonation driven highly efficient H_2O_2 photosynthesis in supramolecular photocatalysts via one-step two-electron oxygen reduction. *Angew. Chem. Int. Ed.* **2025**, *64*, e202421356. DOI PubMed
135. Liu, L.; Gao, M. Y.; Yang, H.; Wang, X.; Li, X.; Cooper, A. I. Linear conjugated polymers for solar-driven hydrogen peroxide production: the importance of catalyst stability. *J. Am. Chem. Soc.* **2021**, *143*, 19287-93. DOI PubMed PMC
136. Sun, J.; Jena, H. S.; Krishnaraj, C.; et al. Pyrene-based covalent organic frameworks for photocatalytic hydrogen peroxide production. *Angew. Chem. Int. Ed.* **2023**, *62*, e202216719. DOI PubMed
137. Wu, S.; Yu, H.; Chen, S.; Quan, X. Enhanced photocatalytic H_2O_2 production over carbon nitride by doping and defect engineering. *ACS Catal.* **2020**, *10*, 14380-9. DOI
138. Liu, P.; Liang, T.; Li, Y.; et al. Photocatalytic H_2O_2 production over boron-doped g-C_3N_4 containing coordinatively unsaturated FeOOH sites and CoO_x clusters. *Nat. Commun.* **2024**, *15*, 9224. DOI PubMed PMC
139. Wu, W.; Li, Z.; Liu, S.; et al. Pyridine-based covalent organic frameworks with pyridyl-imine structures for boosting photocatalytic H_2O_2 production via one-step $2e^-$ oxygen reduction. *Angew. Chem. Int. Ed.* **2024**, *63*, e202404563. DOI PubMed
140. Zhang, Y.; Pan, C.; Bian, G.; et al. H_2O_2 generation from O_2 and H_2O on a near-infrared absorbing porphyrin supramolecular photocatalyst. *Nat. Energy* **2023**, *8*, 361-71. DOI
141. Zhang, Y.; Pan, C.; Li, J.; Zhu, Y. Recent progress in nonsacrificial H_2O_2 generation using organic photocatalysts and *in situ* applications for environmental remediation. *Acc. Mater. Res.* **2024**, *5*, 76-88. DOI
142. Wang, L.; Zhu, W. Organic donor-acceptor systems for photocatalysis. *Adv. Sci.* **2024**, *11*, 2307227. DOI PubMed PMC
143. Singh, J.; Ruda, H. E.; Narayan, M. R.; Ompong, D. Concept of Excitons. In *Optical Properties of Materials and Their Applications*, 2nd ed; John Wiley & Sons, 2019; pp 129-55. DOI
144. Liu, E.; van Baren, J.; Lu, Z.; et al. Exciton-polaron Rydberg states in monolayer $MoSe_2$ and WSe_2. *Nat. Commun.* **2021**, *12*, 6131.

DOI PubMed PMC

145. Chernikov, A.; Berkelbach, T. C.; Hill, H. M.; et al. Exciton binding energy and nonhydrogenic rydberg series in monolayer WS_2. *Phys. Rev. Lett.* **2014**, *113*, 076802. DOI PubMed
146. Elward, J. M.; Chakraborty, A. Effect of dot size on exciton binding energy and electron-hole recombination probability in CdSe quantum dots. *J. Chem. Theory Comput.* **2013**, *9*, 4351-9. DOI PubMed
147. Dvorak, M.; Wei, S. H.; Wu, Z. Origin of the variation of exciton binding energy in semiconductors. *Phys. Rev. Lett.* **2013**, *110*, 016402. DOI PubMed
148. Valencia, A. M.; Bischof, D.; Anhäuser, S.; et al. Excitons in organic materials: revisiting old concepts with new insights. *Electron. Struct.* **2023**, *5*, 033003. DOI
149. Zhu, Y.; Zhao, F.; Wang, W.; Li, Y.; Zhang, S.; Lin, Y. Exciton binding energy of non-fullerene electron acceptors. *Adv. Energy Sustain. Res.* **2022**, *3*, 2100184. DOI
150. Lunt, R. R.; Benziger, J. B.; Forrest, S. R. Relationship between crystalline order and exciton diffusion length in molecular organic semiconductors. *Adv. Mater.* **2010**, *22*, 1233-6. DOI PubMed
151. Zhu, Y.; Zhang, Z.; Si, W.; et al. Organic photovoltaic catalyst with extended exciton diffusion for high-performance solar hydrogen evolution. *J. Am. Chem. Soc.* **2022**, *144*, 12747-55. DOI PubMed
152. Kraner, S.; Scholz, R.; Koerner, C.; Leo, K. Design proposals for organic materials exhibiting a low exciton binding energy. *J. Phys. Chem. C* **2015**, *119*, 22820-5. DOI
153. Shuai, Z.; Geng, H.; Xu, W.; Liao, Y.; André, J. M. From charge transport parameters to charge mobility in organic semiconductors through multiscale simulation. *Chem. Soc. Rev.* **2014**, *43*, 2662-79. DOI PubMed
154. Abdalla, H.; Zuo, G.; Kemerink, M. Range and energetics of charge hopping in organic semiconductors. *Phys. Rev. B* **2017**, *96*, 241202. DOI
155. Coropceanu, V.; Cornil, J.; da Silva Filho, D. A.; Olivier, Y.; Silbey, R.; Brédas, J. L. Charge transport in organic semiconductors. *Chem. Rev.* **2007**, *107*, 926-52. DOI PubMed
156. Giannini, S.; Blumberger, J. Charge transport in organic semiconductors: the perspective from nonadiabatic molecular dynamics. *Acc. Chem. Res.* **2022**, *55*, 819-30. DOI PubMed PMC
157. Schön, J. H.; Kloc, C.; Batlogg, B. Fractional quantum hall effect in organic molecular semiconductors. *Science* **2000**, *288*, 2338-40. DOI PubMed
158. Griggs, S.; Marks, A.; Bristow, H.; McCulloch, I. n-Type organic semiconducting polymers: stability limitations, design considerations and applications. *J. Mater. Chem. C* **2021**, *9*, 8099-128. DOI PubMed PMC
159. Li, H.; Li, H.; Dai, Q.; Li, H.; Brédas, J. L. Hydrolytic stability of boronate ester-linked covalent organic frameworks. *Adv. Theory. Simul.* **2018**, *1*, 1700015. DOI
160. Chen, P.; Dong, X.; Huang, M.; et al. Rapid self-decomposition of g-C_3N_4 during gas-solid photocatalytic CO_2 reduction and its effects on performance assessment. *ACS Catal.* **2022**, *12*, 4560-70. DOI
161. Sugie, A.; Nakano, K.; Tajima, K.; Osaka, I.; Yoshida, H. Dependence of exciton binding energy on bandgap of organic semiconductors. *J. Phys. Chem. Lett.* **2023**, *14*, 11412-20. DOI PubMed PMC
162. Ma, H.; Wei, M.; Jin, F.; Chen, T.; Ma, Y. Two-dimensional COF with rather low exciton binding energies comparable to 3D inorganic semiconductors in the visible range for water splitting. *J. Phys. Chem. C* **2019**, *123*, 24626-33. DOI
163. Lan, Z. A.; Zhang, G.; Chen, X.; Zhang, Y.; Zhang, K. A. I.; Wang, X. Reducing the exciton binding energy of donor-acceptor-based conjugated polymers to promote charge-induced reactions. *Angew. Chem. Int. Ed.* **2019**, *58*, 10236-40. DOI PubMed
164. Dimitriev, O. P. Dynamics of excitons in conjugated molecules and organic semiconductor systems. *Chem. Rev.* **2022**, *122*, 8487-593. DOI PubMed
165. Chen, Y.; Yan, C.; Dong, J.; et al. Structure/property control in photocatalytic organic semiconductor nanocrystals. *Adv. Funct. Mater.* **2021**, *31*, 2104099. DOI
166. Yan, Y.; Yu, X.; Shao, C.; Hu, Y.; Huang, W.; Li, Y. Atomistic structural engineering of conjugated microporous polymers promotes photocatalytic biomass valorization. *Adv. Funct. Mater.* **2023**, *33*, 2304604. DOI
167. Qin, N.; Mao, A.; Li, L.; et al. Construction of benzothiadiazole-based D-A covalent organic frameworks for photocatalytic reduction of Cr (VI) and synergistic elimination of organic pollutants. *Polymer* **2022**, *262*, 125483. DOI
168. Flanders, N. C.; Kirschner, M. S.; Kim, P.; et al. Large exciton diffusion coefficients in two-dimensional covalent organic frameworks with different domain sizes revealed by ultrafast exciton dynamics. *J. Am. Chem. Soc.* **2020**, *142*, 14957-65. DOI PubMed
169. Zhang, X.; Geng, K.; Jiang, D.; Scholes, G. D. Exciton diffusion and annihilation in an sp^2 carbon-conjugated covalent organic framework. *J. Am. Chem. Soc.* **2022**, *144*, 16423-32. DOI PubMed
170. Blätte, D.; Ortmann, F.; Bein, T. Photons, excitons, and electrons in covalent organic frameworks. *J. Am. Chem. Soc.* **2024**, *146*, 32161-205. DOI PubMed PMC
171. Dogru, M.; Handloser, M.; Auras, F.; et al. A photoconductive thienothiophene-based covalent organic framework showing charge transfer towards included fullerene. *Angew. Chem. Int. Ed.* **2013**, *52*, 2920-4. DOI PubMed
172. Jakowetz, A. C.; Hinrichsen, T. F.; Ascherl, L.; et al. Excited-state dynamics in fully conjugated 2D covalent organic frameworks. *J. Am. Chem. Soc.* **2019**, *141*, 11565-71. DOI PubMed
173. Pati, P. B.; Damas, G.; Tian, L.; et al. An experimental and theoretical study of an efficient polymer nano-photocatalyst for hydrogen

evolution. *Energy Environ. Sci.* **2017**, *10*, 1372-6. DOI

174. Wang, G. B.; Xu, H. P.; Xie, K. H.; et al. A covalent organic framework constructed from a donor-acceptor-donor motif monomer for photocatalytic hydrogen evolution from water. *J. Mater. Chem. A* **2023**, *11*, 4007-12. DOI
175. Yang, J.; Jing, J.; Zhu, Y. A full-spectrum porphyrin-fullerene D-A supramolecular photocatalyst with giant built-in electric field for efficient hydrogen production. *Adv. Mater.* **2021**, *33*, 2101026. DOI PubMed
176. Liu, W.; He, C.; Huang, S.; et al. Enhancing carrier transport via σ-linkage length modulation in D-σ-A semiconductors for photocatalytic oxidation. *Angew. Chem. Int. Ed.* **2023**, *62*, e202304773. DOI PubMed
177. Zhang, Z.; Wang, J.; Liu, D.; et al. Highly efficient organic photocatalyst with full visible light spectrum through π-π stacking of TCNQ-PTCDI. *ACS Appl. Mater. Interfaces* **2016**, *8*, 30225-31. DOI PubMed
178. Guo, Y.; Zhou, Q.; Zhu, B.; Tang, C. Y.; Zhu, Y. Advances in organic semiconductors for photocatalytic hydrogen evolution reaction. *EES Catal*. **2023**, *1*, 333-52. DOI
179. Kosco, J.; Bidwell, M.; Cha, H.; et al. Enhanced photocatalytic hydrogen evolution from organic semiconductor heterojunction nanoparticles. *Nat. Mater.* **2020**, *19*, 559-65. DOI PubMed PMC
180. Wadsworth, A.; Hamid, Z.; Kosco, J.; Gasparini, N.; McCulloch, I. The bulk heterojunction in organic photovoltaic, photodetector, and photocatalytic applications. *Adv. Mater.* **2020**, *32*, 2001763. DOI PubMed
181. Cheng, C.; He, B.; Fan, J.; Cheng, B.; Cao, S.; Yu, J. An inorganic/organic S-scheme heterojunction H_2-production photocatalyst and its charge transfer mechanism. *Adv. Mater.* **2021**, *33*, 2100317. DOI PubMed
182. Yang, Y.; Li, D.; Cai, J.; et al. Enhanced photocatalytic hydrogen evolution from organic ternary heterojunction nanoparticles featuring a compact alloy-like phase. *Adv. Funct. Mater.* **2023**, *33*, 2209643. DOI
183. Zhang, Z.; Zhu, Y.; Chen, X.; Zhang, H.; Wang, J. A full-spectrum metal-free porphyrin supramolecular photocatalyst for dual functions of highly efficient hydrogen and oxygen evolution. *Adv. Mater.* **2019**, *31*, 1806626. DOI PubMed
184. Wu, X.; Han, X.; Liu, Y.; Liu, Y.; Cui, Y. Control interlayer stacking and chemical stability of two-dimensional covalent organic frameworks via steric tuning. *J. Am. Chem. Soc.* **2018**, *140*, 16124-33. DOI PubMed
185. Ma, Y.; Wang, Y.; Li, H.; et al. Three-dimensional chemically stable covalent organic frameworks through hydrophobic engineering. *Angew. Chem. Int. Ed.* **2020**, *59*, 19633-8. DOI PubMed
186. Khalil, I. E.; Das, P.; Thomas, A. Two-dimensional covalent organic frameworks: structural insights across different length scales and their impact on photocatalytic efficiency. *Acc. Chem. Res.* **2024**, *57*, 3138-50. DOI PubMed PMC
187. Li, X.; Cai, S.; Sun, B.; Yang, C.; Zhang, J.; Liu, Y. Chemically robust covalent organic frameworks: progress and perspective. *Matter* **2020**, *3*, 1507-40. DOI
188. Li, P.; Fang, J.; Wang, Y.; et al. Synergistic effect of dielectric property and energy transfer on charge separation in non-fullerene-based solar cells. *Angew. Chem. Int. Ed.* **2021**, *60*, 15054-62. DOI PubMed
189. Li, Z.; He, T.; Gong, Y.; Jiang, D. Covalent organic frameworks: pore design and interface engineering. *Acc. Chem. Res.* **2020**, *53*, 1672-85. DOI PubMed
190. He, T.; Zhao, Y. Covalent organic frameworks for energy conversion in photocatalysis. *Angew. Chem. Int. Ed.* **2023**, *62*, e202303086. DOI PubMed
191. Nagai, A.; Guo, Z.; Feng, X.; et al. Pore surface engineering in covalent organic frameworks. *Nat. Commun.* **2011**, *2*, 536. DOI PubMed
192. Liu, R.; Chen, Y.; Yu, H.; et al. Linkage-engineered donor-acceptor covalent organic frameworks for optimal photosynthesis of hydrogen peroxide from water and air. *Nat. Catal.* **2024**, *7*, 195-206. DOI
193. Xu, H.; Chen, X.; Gao, J.; et al. Catalytic covalent organic frameworks via pore surface engineering. *Chem. Commun.* **2014**, *50*, 1292-4. DOI PubMed
194. Kang, X.; Stephens, E. R.; Spector-Watts, B. M.; et al. Challenges and opportunities for chiral covalent organic frameworks. *Chem. Sci.* **2022**, *13*, 9811-32. DOI PubMed PMC
195. Han, X.; Yuan, C.; Hou, B.; et al. Chiral covalent organic frameworks: design, synthesis and property. *Chem. Soc. Rev.* **2020**, *49*, 6248-72. DOI PubMed
196. Fang, Q.; Zhuang, Z.; Gu, S.; et al. Designed synthesis of large-pore crystalline polyimide covalent organic frameworks. *Nat. Commun.* **2014**, *5*, 4503. DOI PubMed
197. Liu, Y.; Zhou, Q.; Yu, H.; et al. Increasing the accessibility of internal catalytic sites in covalent organic frameworks by introducing a bicontinuous mesostructure. *Angew. Chem. Int. Ed.* **2024**, *63*, e202400985. DOI PubMed
198. Spitler, E. L.; Koo, B. T.; Novotney, J. L.; et al. A 2D covalent organic framework with 4.7-nm pores and insight into its interlayer stacking. *J. Am. Chem. Soc.* **2011**, *133*, 19416-21. DOI PubMed
199. Jin, S.; Ding, X.; Feng, X.; et al. Charge dynamics in a donor-acceptor covalent organic framework with periodically ordered bicontinuous heterojunctions. *Angew. Chem. Int. Ed.* **2013**, *52*, 2017-21. DOI PubMed
200. Banerjee, T.; Lotsch, B. V. The wetter the better. *Nat. Chem.* **2018**, *10*, 1175-7. DOI PubMed